# THE INFLUENCE OF THE MUGESE SHEAR ZONE STRUCTURES ON STRAIN ACCOMMODATION IN THE NORTHERN MALAWI RIFT

By

SAM MICHAEL DAWSON

Bachelor of Science in Geology

University of North Carolina at Chapel Hill

Chapel Hill, NC

2014

Submitted to the Faculty of the
Graduate College of the
Oklahoma State University
in partial fulfillment of
the requirements for
the Degree of
MASTER OF SCIENCE
December, 2016

THE INFLUENCE OF THE MUGESE SHEAR ZONE STRUCTURES ON STRAIN ACCOMMODATION IN THE NORTHERN MALAWI RIFT

Thesis Approved:

Dr. Daniel Laó Dávila

Thesis Adviser

Dr. Mohamed Abdelsalam

Dr. Estella Atekwana

ACKNOWLEDGEMENTS

I would like to thank Patrick Chindandali, Bryan Clappe, Courtney Hull, Tiara Johnson, Victor Nyalugwe, Kennedy, and Faison for their assistance collecting data in the field. I would also like to thank Jalf Salima and the Geological Survey of Malawi for their collaboration. Thank you to my committee for their help with this project. Thank you to Devon Energy for providing me with a fellowship. This material is based upon work supported by the National Science Foundation under grant no. II – 1358150.

Name: Sam Dawson

Date of Degree: December, 2016

Title of Study: THE INFLUENCE OF THE MUGESE SHEAR ZONE STRUCTURES ON STRAIN ACCOMMODATION IN THE NORTHERN MALAWI RIFT

Major Field: GEOLOGY

Abstract:

The Livingstone border fault, with its 7 km of maximum displacement, accommodates most of the extension in the northern portion of the N-striking Malawi Rift (the southern segment of the Western Branch of the East African Rift System (EARS)) through the development of an E-dipping half-graben. However, the 2009 earthquake sequence in the greater Karonga area, west of the Livingstone border fault, suggests that extension is also being accommodated in the hanging-wall of the half-graben. This hanging wall block is underlain in part by the NW- and N-striking Precambrian Mugese Shear Zone (MSZ) and N-striking Karoo-age (Paleozoic – Mesozoic) rift structures. We used aeromagnetic data to map the Precambrian macro-scale structural fabric of the greater Karonga region. Moreover, we mapped mesoscopic-scale structures within the Precambrian and younger rocks in the region. Additionally, we used Shuttle Radar Topography Mission (SRTM) Digital Elevation Models (DEM) to map rift-related brittle structures. We found that in the northern portion of the Karonga Fault Zone, a fault zone that accommodates the majority of extension in this region, one major fault is oriented 32°/ 59° SE which cuts across the Precambrian foliation that has an orientation of 301°/ 79° NE. South of the city of Karonga, the Precambrian foliation is sub-vertical and has a strike of 321°. Here, the Karonga fault splays from a main fault with a 2 km damage zone to several distinct E-and W-dipping faults over a 10 km zone that strike in the general direction of the foliation planes of the MSZ. The N-striking Karoo rift horsts and grabens and their associated rock formations might have also been reactivated in this area. These relationships suggest that within the northern Malawi Rift, extension was accommodated differently based on the nature and orientation of the pre-existing structures. The Precambrian and Paleozoic-Mesozoic structural fabric underlying the southern portion of the Karonga Fault Zone favors accommodation of slip along pre-existing planes, whereas strain is localized in a narrow zone in the northern portion of the fault zone and is not accommodated through reactivation of pre-existing structures.

TABLE OF CONTENTS

Chapter Page

I. INTRODUCTION .....1

II. REVIEW OF LITERATURE.....9

The Tectonic Setting.....9
The Mugese Shear Zone and Associated Precambrian Features .....10
Paleozoic-Mesozoic Karoo Rifting.....11
Slip along Pre-Existing Structures.....12
The Karonga Fault Zone .....13

III. METHODOLOGY .....15

Remote Sensing Analysis .....15
Aeromagnetic Analysis.....16
Meso-Scale Structural Analysis.....19

IV. RESULTS.....21

Structural Domains .....21
Domain A.....21
Domain B.....26
Domain C.....27
Domain D.....29
Domain E .....30
Domain F .....31
Domain G.....32
Fault Characteristics from Remote Sensing.....34
Aeromagnetic Data .....34

V. DISCUSSION & CONCLUSIONS.....35

Interpreting Basement Fabric through Aeromagnetic Data.....35
Strain Accommodation .....36
Implications for Seismic Hazard.....38
Conclusions.....39

REFERENCES .....41

Chapter Page

APPENDICES .....48

Appendix A .....48
Table of Foliation Orientations .....48
Table of Bedding Orientations .....50
Table of Shear Zones .....51
Table of Fault Orientations .....51

LIST OF FIGURES

Figure Page

1. Tectonic Setting of the Malawi Rift....2

2. Geologic Map of Orogenic Belts Surrounding the Malawi Rift....4

3. Geologic Map of the Greater Karonga Area....6

4. Seismisity Map of the Greater Karonga Area....8

5. Aeromagnetic Derivative Map of Mugese Shear Zone Foliations....17

6. Aeromagnetic Tilt Map of the Greater Karonga Area....20

7. Explanation of the Likelihood of Reactivation for the Stereonets....21

8. Summary of Domain A....23

9. Field Pictures....24

10. Summary of Domain B....27

11. Summary of Domain C....28

12. Summary of Domain D....30

13. Summary of Domain E....31

14. Summary of Domain F....32

15. Summary of Domain G....33

16. Hanging-Wall Transect....38

# CHAPTER I

## INTRODUCTION

Lithospheric-scale suture zones and other pre-existing structures such as major shear zones have long been recognized as important elements of strain localization during the early stages of the development of continental rifts (McConnell 1972, Morley et al. 2004, Morley 2010, Katumwehe et al. 2015a). While numerical models have been able to explain strain localization due to asthenospheric upwelling in magma-rich rifts (Buck 2006), localization of strain during incipient continental rifting in magma-poor areas such as the Malawi Rift is not equally well understood. There are compelling examples of pre-existing weaknesses exerting control over strain localization in a variety of rift settings including the Main Ethiopian Rift, rift basins in Thailand, and the Albertine and Rhino grabens of Uganda (e.g. Korme et al. 2004; Morley et al 2004; Keranen and Klemperer 2008; Katumwehe et al. 2015a). Models of listric fault development have shown that strain is accommodated in the hanging-wall as the listric fault matures (e.g. Cloos 1968, Withjack et al. 1995), though it is not clear what controls the localization of strain in the hanging-wall of continental rifts. We are seeking to answer how the orientation of pre-existing structures (both Precambrian crystalline basement and Paleozoic-Mesozoic rifts) relative to the stress field in the western flank of the North Basin of the Malawi Rift (the

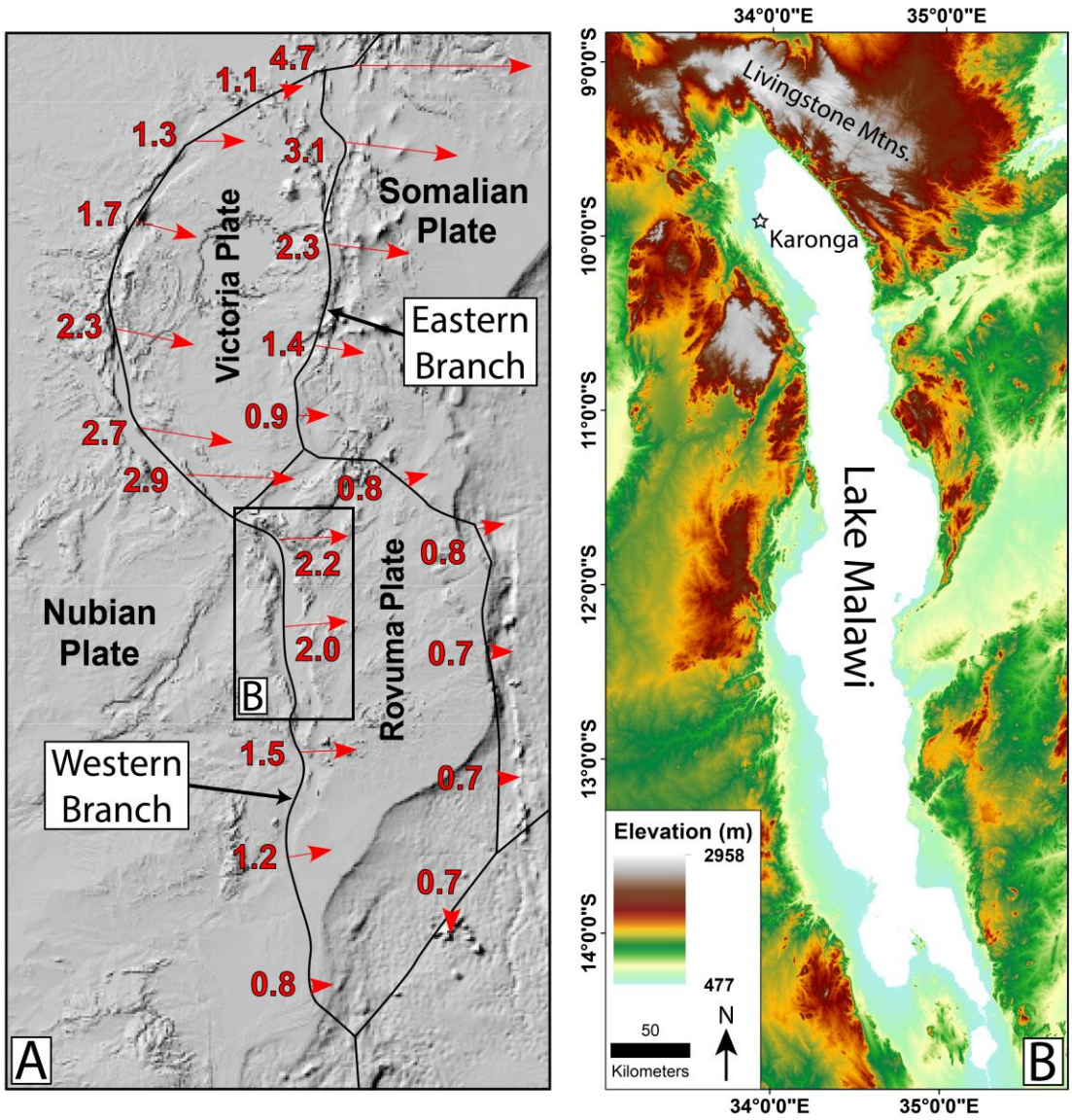


Figure 1. (a) Tectonic setting of the Malawi Rift(modified from Laó-Dávila et al. 2015), and modeled rift opening velocities from Saria et al. (2014). Rates are given in mm/yr. The northern portion of the rift is currently separating the Nubian and Rovuma Plates at 2.2 mm/yr towards N85E. (b) Shuttle Radar Topography Mission (SRTM) Digital Elevation Model (DEM) of the Malawi Rift.

southern extension of the Western Branch of the East African Rift System (EARS)) affect strain localization for this area. Studying how new rift faults form away from border faults is key to understanding their role in strain accommodation and assessing the seismic hazard of these areas. Our focus site is the greater Karonga area (Figs. 1 – 3), which is prone to seismic activity. This is evidenced by the 2009 sequence containing

four $M_w$5.4 – 5.9 earthquakes with moment tensor solutions showing ENE – WSW extension (Fig. 4; Biggs et al. 2010; Macheyeki et al. 2015). A greater understanding of the strain accommodation in new and magma-poor rifts can help to mitigate the seismic hazard here as well as contribute to our knowledge of strain accommodation in magma-poor rifts. If the pre-existing structural fabric in the hanging wall of the Livingstone border fault serves as planes of weakness, the areas near strongly-foliated basement rocks are at risk of further seismicity.

The greater Karonga area is a relatively young portion of the Western Branch of the EARS. The Malawi Rift in this region extends within Precambrian crystalline rocks dominated by the NW- to NNW-striking Mugese Shear Zone (MSZ) as well as N-striking Karoo rifts. These pre-existing structures have the potential to accommodate strain in the hanging-wall of the Livingstone border fault. To measure this effect, 1) we mapped brittle structures with Shuttle Radar Topography Mission (SRTM) Digital Elevation Models (DEM), 2) we mapped the ductile structures of the MSZ with aeromagnetic data,

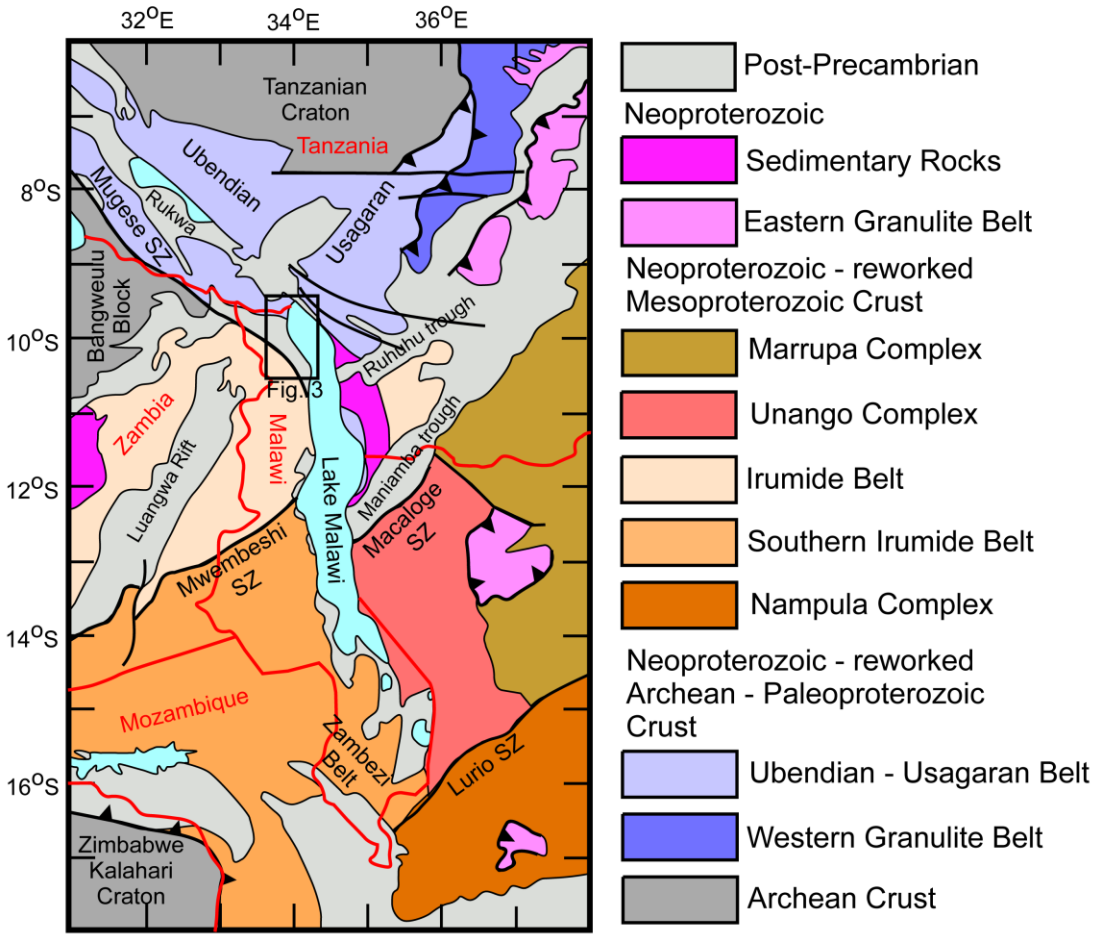


Figure 2. Geological map of Malawi and surrounding showing the orogenic belts around the Malawi Rift. The Malawi Rift is located within Precambrian belts and Karoo rifts. The Mugese Shear Zone is exposed on the northwest part of the Malawi Rift. The black rectangle shows the area of Figure 3. Modified from Fritz et al. (2013).

3) we extracted structural orientations from a field campaign, and 4) we compared the orientations of the pre-existing structures with the current and initial stress regimes. Our objective is to characterize the interaction of rift-related faults with the Precambrian fabric in our study area. Comparing these structures to the modern stress field will show if the pre-existing weaknesses are likely to have reactivated. For the purposes of this paper, we consider a foliation plane to be "reactivated" if there has likely been slip along that plane. Ring (1994) concluded from mesoscopic structural analyses of outcrops within

the North Basin of the Malawi Rift that the Precambrian basement fabric in this area has not been reactivated by accommodating strain during the onset of the Malawi Rift. Nonetheless, new aeromagnetic data collected by the Government of Malawi and presented in this study (that allowed us to see the general trends of the basement fabric) suggest that some map-scale structural trends within the MSZ are at a suitable orientation to reactivate and localize strain. Hence, the scale dependency of observation (map-scale vs mesoscopic-scale) may account for the difference in interpretation between Ring (1994) and this study.

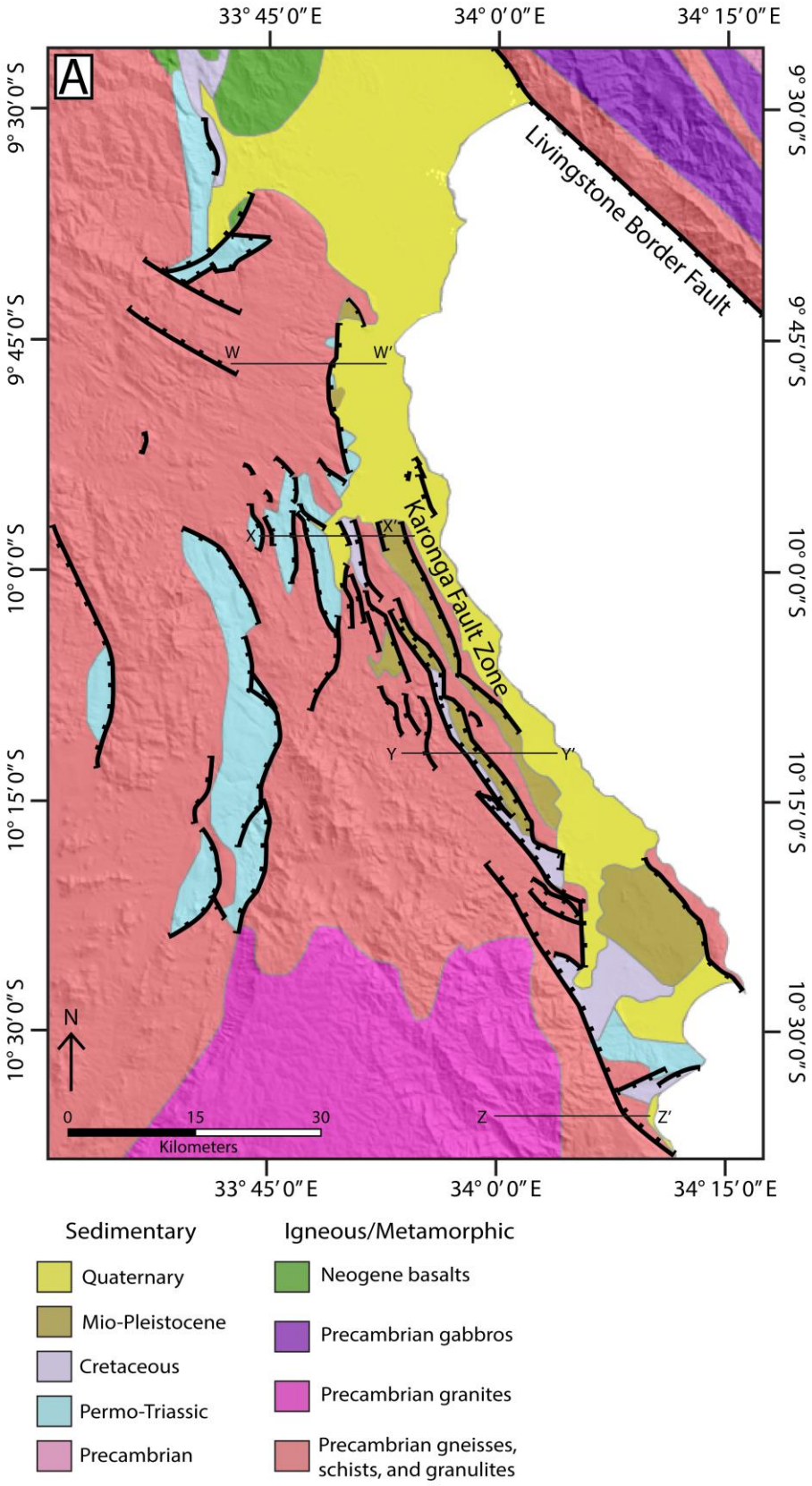
33° 45′ 0″ E
34° 0′ 0″ E
34° 15′ 0″ E
9° 30′ 0″ S
9° 45′ 0″ S
10° 0′ 0″ S
10° 15′ 0″ S
10° 30′ 0″ S
A
Livingstone Border Fault
Karonga Fault Zone
W
W′
X
X′
Y
Y′
Z
Z′
N
0
15
30
Kilometers
Sedimentary
Quaternary
Mio-Pleistocene
Cretaceous
Permo-Triassic
Precambrian
Igneous/Metamorphic
Neogene basalts
Precambrian gabbros
Precambrian granites
Precambrian gneisses, schists, and granulites

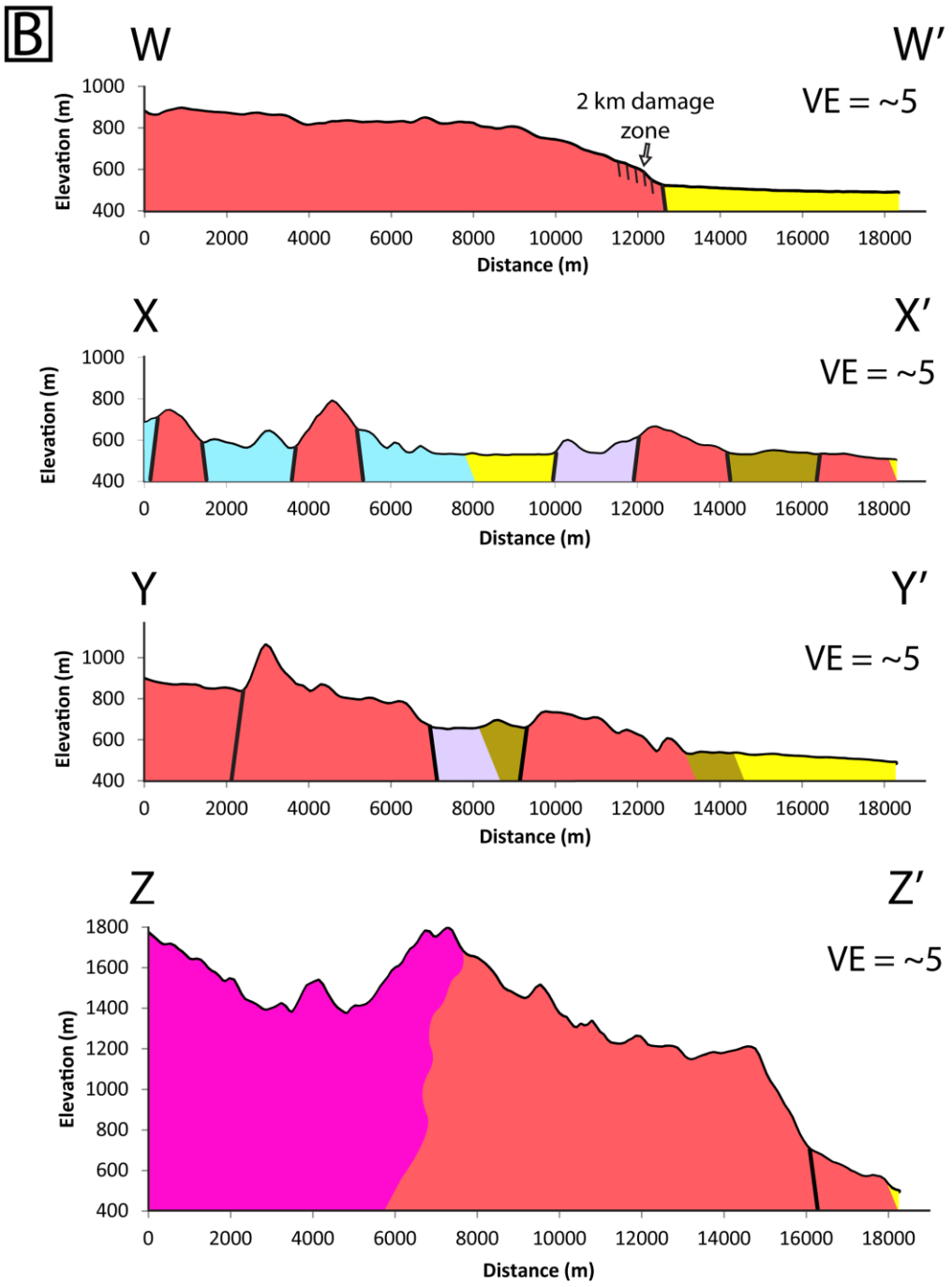


Figure 3. (a) Geologic map of the northwest Malawi Rift in the Karonga area. This area shows part of the hanging wall of the Livingstone border fault. Modified from Geological Survey of Malawi (1966) and Biggs et al. (2010). (b) Cross-sections W–W' and Z–Z' show a fault accommodating the strain in these areas, whereas X–X' and Y–Y' have several faults that accommodate the strain.

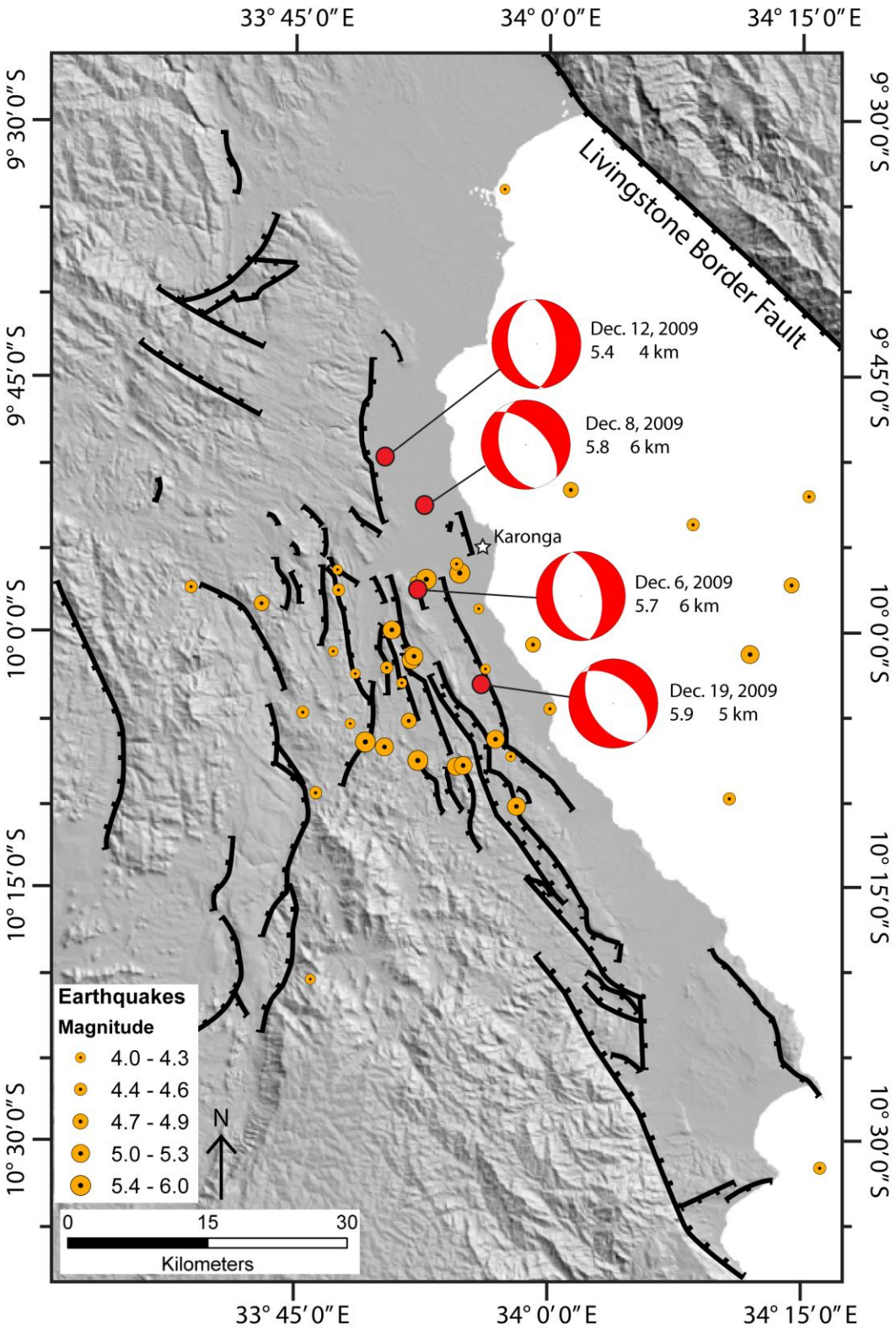


Figure 4. Map of faults and earthquake epicenters since 1901 for earthquakes of magnitude 4.0 or greater in the Karonga area. The locations of epicenters coincides with the region of distributed strain along several fault planes in latitudes 9° 55’ to 10° 10’. Orange epicenters are from United States Geological Survey (2016), and red epicenters are from Biggs et al. (2010).

# CHAPTER II

# REVIEW OF LITERATURE

## *The Tectonic Setting*

The Malawi Rift is the 650 km long, 60 km wide rift that represents the southern segment of the Western Branch of the EARS (Fig. 1). It was initiated in the late Miocene-Pleistocene and extension is still going on as evidenced by the frequency of seismic activity. This makes the Malawi Rift an ideal area to study a developing continental rift (Chorowicz 2005). The rift flanks are highest in the northern portion of the rift, particularly at the Livingstone Mountains, which have a prominence of close to 2.5 km above Lake Malawi (Fig. 1b). The northernmost tip of the Malawi Rift is separating the Nubian and Rovuma Plates in an E-W direction at 2.2 mm per year, while the southernmost separation is extending E-W at 0.8 mm per year (Fig. 1a, Saria et al. 2014).

Laó-Dávila et al. (2015) showed that that the Malawi Rift can be divided into three first order morphologically-distinct segments that include the Northern, Central, and Southern segments. The focus of this study, the greater Karonga area, lies within the Northern segment which is characterized by the presence of ~150 km border faults (representing second order segmentation) that alternate between the western and eastern flanks of the rift. Together with the Livingstone border fault in the east, the Karonga

Fault Zone to the west represents the northernmost second-order segment of the Malawi Rift. This second order segment forms an east-dipping half-graben transitioning southward into an asymmetrical graben (Lao Davila et al., 2015).

*The Mugese Shear Zone and Associated Precambrian Features*

Precambrian crystalline rocks constitute the pre-rift formations within which the Malawi Rift extends (Fig. 2; Laó-Dávila et al. 2015). The northern part of the Malawi Rift stretches within Archean to Mesoproterozoic crust that has been variably reworked during the Neoproterozoic (Fritz et. al. 2013). The northeastern flank of the rift is dominated by the Archean-Paleoproterozoic Usagaran Orogenic Belt (Fig. 2). The Archean-Paleoproterozoic Ubendian Orogenic Belt is found northwest of the rift extending between the Tanzanian Craton and the Bangweulu Block (Fig. 2). The Mesoproterozoic Southern Irumide orogenic belt crops out in the southwestern side of the northern segment of the Malawi Rift separated from the Ubendian orogenic belt by the MSZ. The Precambrian basement rocks have strong structural fabric trends developed from previous contractional tectonic regimes due to convergence of different Precambrian blocks (Morley et al. 2010). Near Karonga, the MSZ contains steeply-dipping foliations that formed during the 580–550 Ma contractional movement between the Irumide and Ubendian Belts (Ring et al. 2002, Fritz et al. 2013). Previous studies suggested that the MSZ had witnessed sinistral strike-slip movement possibly during the late stage of its tectonic evolution (Ring et al., 2002). In the gneissic rocks, biotite, quartz, and feldspars define the foliations together with accessory minerals including sillimanite, garnet, and hornblende (Ring et al. 2002). Amphibolites are also common in

the MSZ, which have schistosity planes defined by horneblende, biotite, feldspar, and garnets.

*Paleozoic-Mesozoic Karoo Rifting*

Predominantly NE-striking Karoo rifts have been reported on both sides of the Malawi Rift, including the Luangwa Rift, Ruhuhu Trough, and Maniamba Trough (Fig. 2). The formation of these rifts is attributed to the fragmentation of Gondwana (Delvaux 2001). Near the greater Karonga area, however, Paleozoic, Mesozoic, and Cenozoic to Quaternary sedimentary rocks can be found in N-striking rift-related basins (Fig. 3a, Laó-Dávila et al. 2015). The Late Carboniferous to Early Triassic Karoo Rift System created N-striking rift basins near Karonga (Fig. 3, Delvaux 2001). These basins were formed in response to stresses created by the Cape fold belt and are typically comprised of half-graben structures that span across Central Africa (Daly et al. 1989). The faults that bound these basins also serve as pre-existing weaknesses that may have slipped during the formation of the Malawi Rift.

*Slip along Pre-Existing Structures*

The control of pre-existing structures of basement rocks on extensional faulting has been well-documented (e.g. Korme et al. 2004, Morley et al. 2004, Espurt et al. 2012, Katumwehe et al. 2015a). Pre-existing structures have been shown to influence slip direction by relocating strain along planes in different directions than the idealized directions predicted for a homogenous material (Coulomb 1776, Mohr 1900, Anderson 1951, Morley et al. 2004, Tingay et al. 2010). Morley et al. (2004) showed in numerical

Coulomb failure models that weak planes have a high likelihood of normal slip if their poles are within 30° trend and 10° plunge of the orientation of the maximum tensile stress.

Basement heterogeneities along the Malawi rift have been suggested to control its escarpment strike and height (Laó Dávila et al. 2015). These heterogeneities are primarily mylonitic fabric in the gneiss and amphibolite facies rocks of the MSZ (Ring et al. 2002). Foliations have been shown to be planes of weakness sufficient for slip (Coussement et al., 1994). Morley (2010) interpreted the orientation of Precambrian fabrics in the EARS, showing that the NW-SE-striking, steeply-dipping foliations of the Ubendian orogenic belt has a high likelihood of slip. The hanging-wall of the Livingstone border fault lies within the Ubendian orogenic belt (Laó Dávila et al. 2015), so that rift structures would take advantage of these planes of weakness.

It is currently unknown how the hanging-wall of the Livingstone border fault (Fig. 1b) of the Malawi Rift is accommodating strain. Scholz and Contreras (1998) showed that border faults in magma-poor rifts cannot continue accommodating extension indefinitely. Rather, new fault systems will develop in response to extension when the original border faults reach a threshold of maximum slip amount and length. Fault modeling of the Livingstone border fault suggests that it has reached its maximum length and slip (Scholz and Contreras 1998, and references therein). The record of seismicity in the greater Karonga area shows earthquake epicenters proximal to mapped faults (Fig. 4, Biggs et al. 2010), suggesting that the hanging-wall of the Livingstone border fault might be accommodating the majority of extension at this stage of rifting in the northern portion of the Malawi Rift. We have termed this structure the Karonga Fault Zone.

*The Karonga Fault Zone*

From the analysis of remote sensing and fault slip data, Ring et al. (1992) suggested a multi-phase stress and slip directions model for the North Basin, which is defined as the portion of the Malawi Rift that extends northward from the intersection of the rift with the Ruhuhu trough (Fig. 2). Mortimer et al. (2007) suggested that the North Basin of the Malawi Rift is separated from a Central Basin by an ENW-trending accommodation zone. Ring et al. (1992) proposed that since ~8 Ma, the direction of extension resulting in the opening of the Malawi Rift has rotated first from ENE to E and second from E to SE. This resulted in both orthogonal and oblique rifting across the Malawi Rift. Saria et al. (2014) predicted from rigid plate model constrained by earthquake focal mechanism and sparse Global Positioning System (GPS) observation that the current opening direction in the northern portion of the Malawi Rift is oriented N85°E. Slip on faults developed in association with the opening of the northern part of the Malawi Rift varies relative to their orientation and location. However, a generalized interpretation suggests initial NE to ENE-striking normal faulting developed during orthogonal rifting (Ring et al. 1992). The second event, that occurred during oblique rifting, created new strike-slip faults as well as accommodating strain by reactivating the pre-existing normal faults into dextral strike-slip faults. Further, strike-slip, normal, and reverse faults developed along primarily new fault surfaces in the most recent event (Ring et al. 1992).

Models suggested for the north basin agree in its development as an E-dipping half-graben with the Livingstone in the eastern side of the Malawi Rift representing the

border fault (Biggs et al., 2010). This geometry predicts the presence of a hinge zone in the western side of the greater Karonga area. Hence, this geometry considers the entire block that stretches from this hinge zone to the Livingstone border fault as the hanging-wall of the half-graben. Earthquake epicenters in the proximity hanging-wall faults of the Livingstone border fault (Fig. 4) show that this area is actively deforming. Biggs et al. (2010) calculated the depths of hypocenters of the 2009 earthquake sequence to be in the range of 4–6 km. The earthquake focal mechanisms are consistent with an ENE – WSW modern extensional direction (Fig. 4, Biggs et al. 2010).

# CHAPTER III

# METHODOLOGY

## *Remote Sensing Analysis*

A Shuttle Radar Topography Mission (SRTM) Digital Elevation Model (DEM) at 90 m spatial resolution was used to map the spatial extent of Malawi Rift-related faults in the greater Karonga area. Faults that have morphological expression appear in hillshade SRTM DEMs as linear features separating terrains with different elevations and that these features can be easily distinguished from the surrounding area (Laó-Dávila et al. 2015). To map morphologically-defined faults that have different orientations, we generated hillshade SRTM DEMs with a sun elevation of 45° and sun azimuth angles of 45° (Fig. 4) and 315°. This allowed us to map major structural trends in the greater Karonga area. We integrated our structural map with the Geological Survey of Malawi (1966) and Biggs et al. (2010) maps that show the spatial distribution of different lithological units to produce a detailed geological map for the greater Karonga area (Fig. 3a). Additionally, to highlight along-strike variation of the rift-related structures, we used the geological map together with topographic profiles extracted from the SRTM DEM to construct E-W geological cross-sections across major structures (Fig. 3b).

*Aeromagnetic Analysis*

Aeromagnetic data was collected by the Government of Malawi in 2013 through NE-SW transects with 250 m spacing between flight paths, 2.5 km tie lines, and a constant terrain clearance of 60 m. The data was processed with edge-detection filters in Geosoft Oasis Montaj and used to create a structural map of the regional Precambrian fabric (Fig. 5). The Precambrian fabric shows up as strong linear magnetic anomalies that were enhanced using upward continuation and horizontal derivative filters, as accomplished by Dhaoui et al. (2014) and Katumwehe et al. (2015a). We chose a total horizontal derivative filter to map basement structures because edge-detection filters are the most successful at enhancing these features (Fairhead et al. 2011).

Stereonets of foliation planes from the aeromagnetic data were extracted following the methods of Katumwehe et al. (2015b). This involved creating a tilt map (Fig. 6) and extracting tilt values every 200 m perpendicular to the regional strike of the magnetic lineations. The corresponding strikes of magnetic structures were measured in Adobe Illustrator and plotted on stereonets.

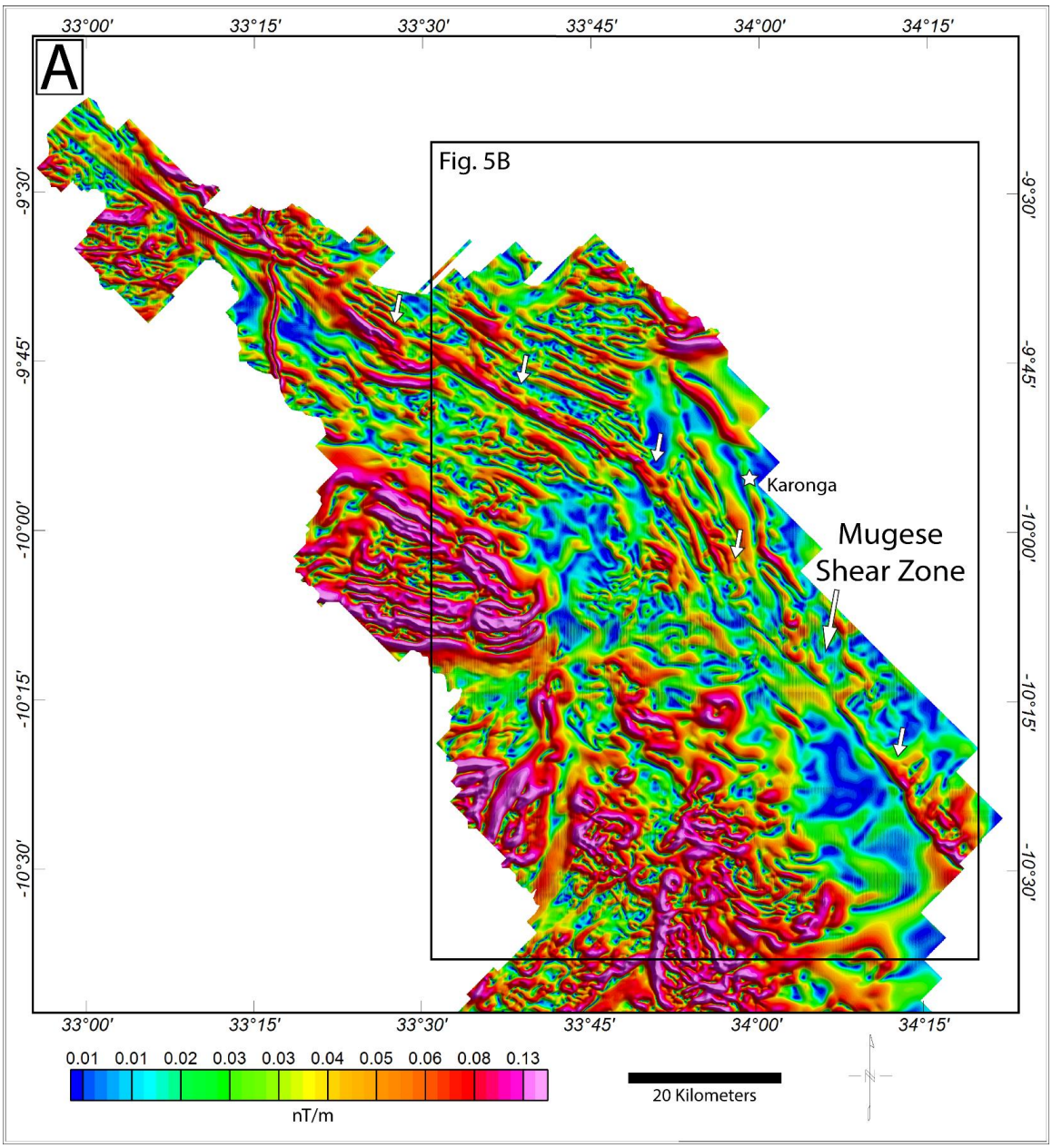
A
Fig. 5B
Karonga
Mugese
Shear Zone
33°00'
33°15'
33°30'
33°45'
34°00'
34°15'
-9°30'
-9°45'
-10°00'
-10°15'
-10°30'
0.01 0.01 0.02 0.03 0.03 0.04 0.05 0.06 0.08 0.13
nT/m
20 Kilometers

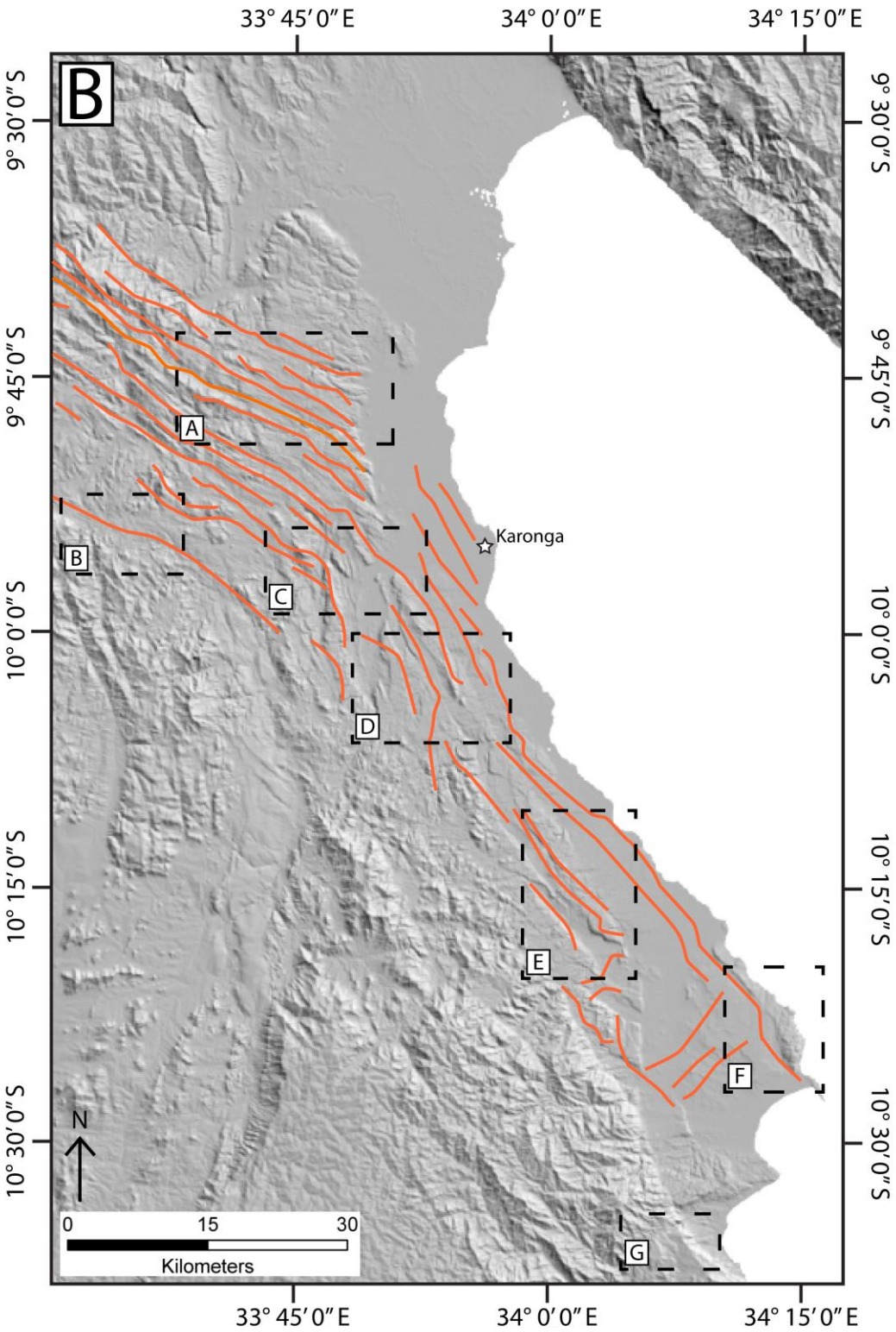


Figure 5. (a) Total horizontal derivative of aeromagnetic data after a 500 m upward continuation. The government of Malawi acquired this data in 2013 with a line spacing of 250 m, 2.5 km tie lines, and a terrain clearance of 60 m. The white arrows denote the Mugese Shear Zone. (b) Lineations mapped from the aeromagnetic data, showing areas with strong regional foliations of the Mugese Shear Zone. Dashed rectangles show the domains used in Figures 8 and 10 – 15.

*Meso-Scale Structural Analysis*

We conducted a field mapping campaign to collect structural and lithological data in the greater Karonga area. We measured the orientation of layering, faults, foliations, folds, and lineations. We determined the sense of movement of faults based on layer offset, drag folds, and mineral steps on fault surfaces. We also noted the confidence level in determining the slip directions, amount of offsets, and the lengths of the fault traces. We determined fault slip following the methods of Marrett and Allmendinger (1990), Doblas (1998), and Sperner and Zweigel (2010). We compared the orientation of the foliations measured in the field with the orientations of foliations derived from the aeromagnetic data. The structural data were grouped into structural domains based on our field measurement locations and on the local orientation of Precambrian basement foliations seen in the aeromagnetic data (Fig. 5). The data for each structural domain were plotted in equal-angle lower hemisphere stereographic projections using Stereonet 9 (Fig. 6; Allmendinger et al. 2012, Marrett and Allmendinger 1990).

Following the work of Morley et al. (2004), we created a template with contours to indicate three different likelihoods (high, moderate, and low) for reactivation of the foliation planes in each domain (Fig. 7). There are two sets of contours to incorporate the initial and modern extensional directions in the Northern Malawi Rift.

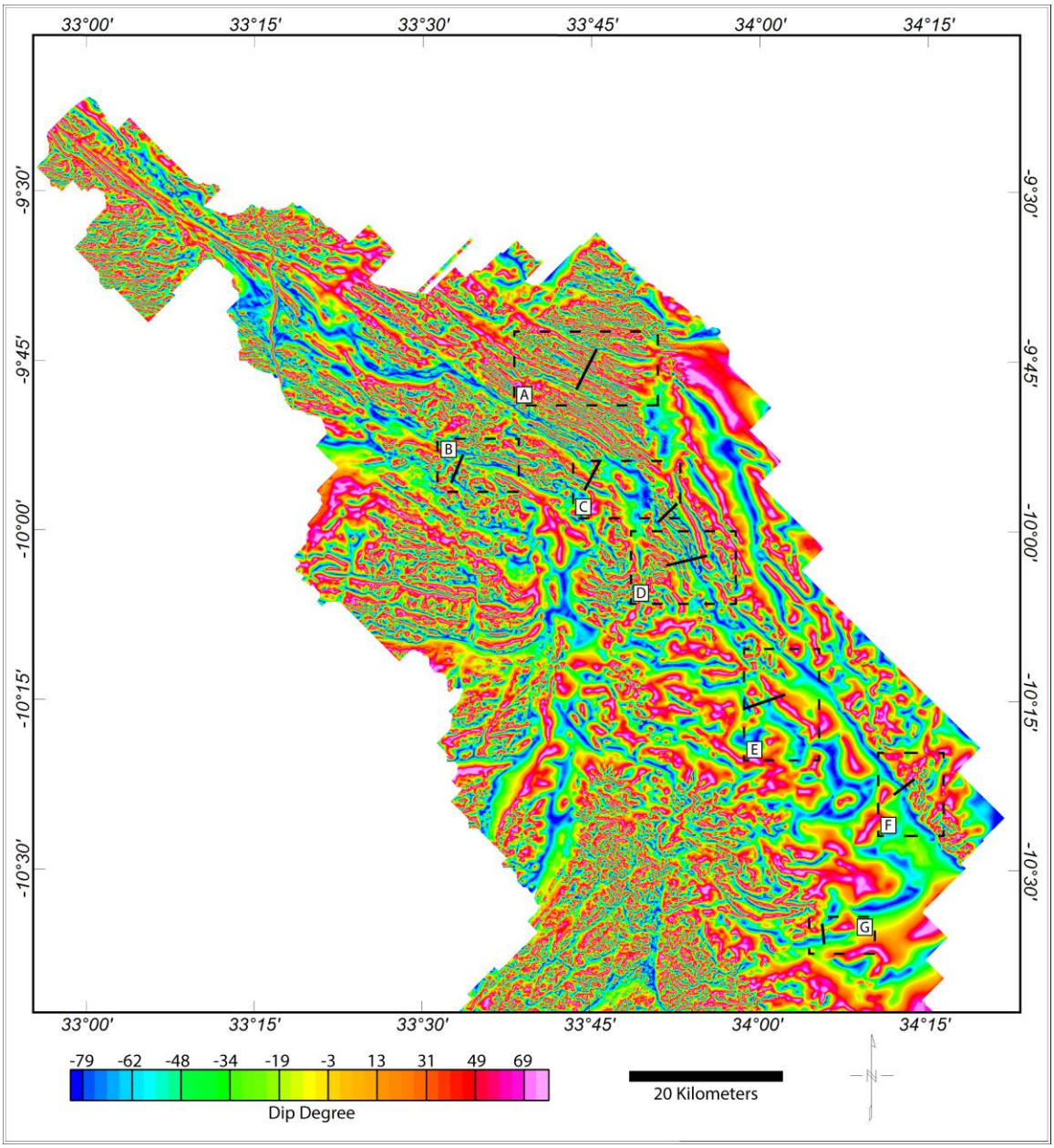


Figure 6. Tilt map of the aeromagnetic data. The black lines are where we sampled the map for dip directions shown in the stereonets showing foliation orientations measured from the aeromagnetic data for each domain. The software we used to generate this map, Oasis Montaj, displays blue, green, and yellow colors to show magnetic structures dipping to the west, while orange, red and pink colors show magnetic structures dipping to the east.

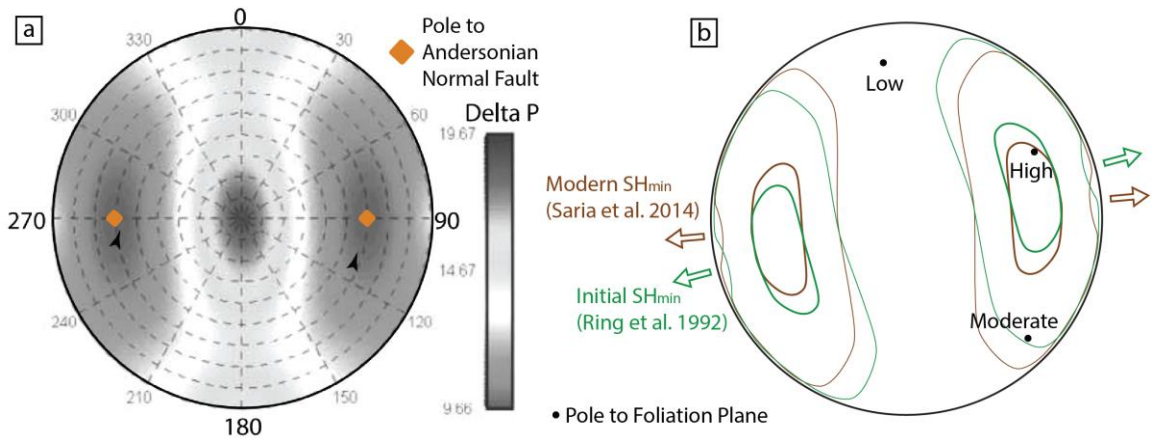


Figure 7. a) Likelihood of reactivation for pre-existing structures in an E-W extensional stress regime. The dark gray region surrounding the pole to the Andersonian normal fault indicates a high likelihood of reactivation (low Delta P, which is the amount of stress required for slip along that plane). b) Contours indicating the three different likelihoods (high, moderate, low) of reactivation traced from (a) and oriented to reflect the initial and modern extensional direction of the Northern Malawi Rift. Modified from Morley et al. (2004).

# CHAPTER IV

# RESULTS

## *Structural Domains*

To analyze the relationship between the Precambrian structure of the MSZ and the Karoo rifts on the one hand and the structure associated with Malawi Rift in the greater Karonga area on the other hand, we divided the study area into seven structural domain titled Domains A through G. This grouping was done based on the orientation and spatial distribution of major structures as mapped from the SRTM DEM and aeromagnetic data and orientation clustering (or lack of it) of mesoscopic structures. Below we describe each domain.

### *Domain A*

Domain A is characterized by basement rocks with an average foliation strike of 301° as measured by the aeromagnetic data that terminate at a single fault escarpment oriented 32°/ 59° E. As measured in the field, there is a 2 km damage zone with normal faults that are predominantly synthetic to the escarpment as shown in cross-section W-W' (Fig. 3b). Both Karoo and Malawi Rift sediments lie adjacent to this ~20 km fault. Foliation measurements from the field align well with those measured from the

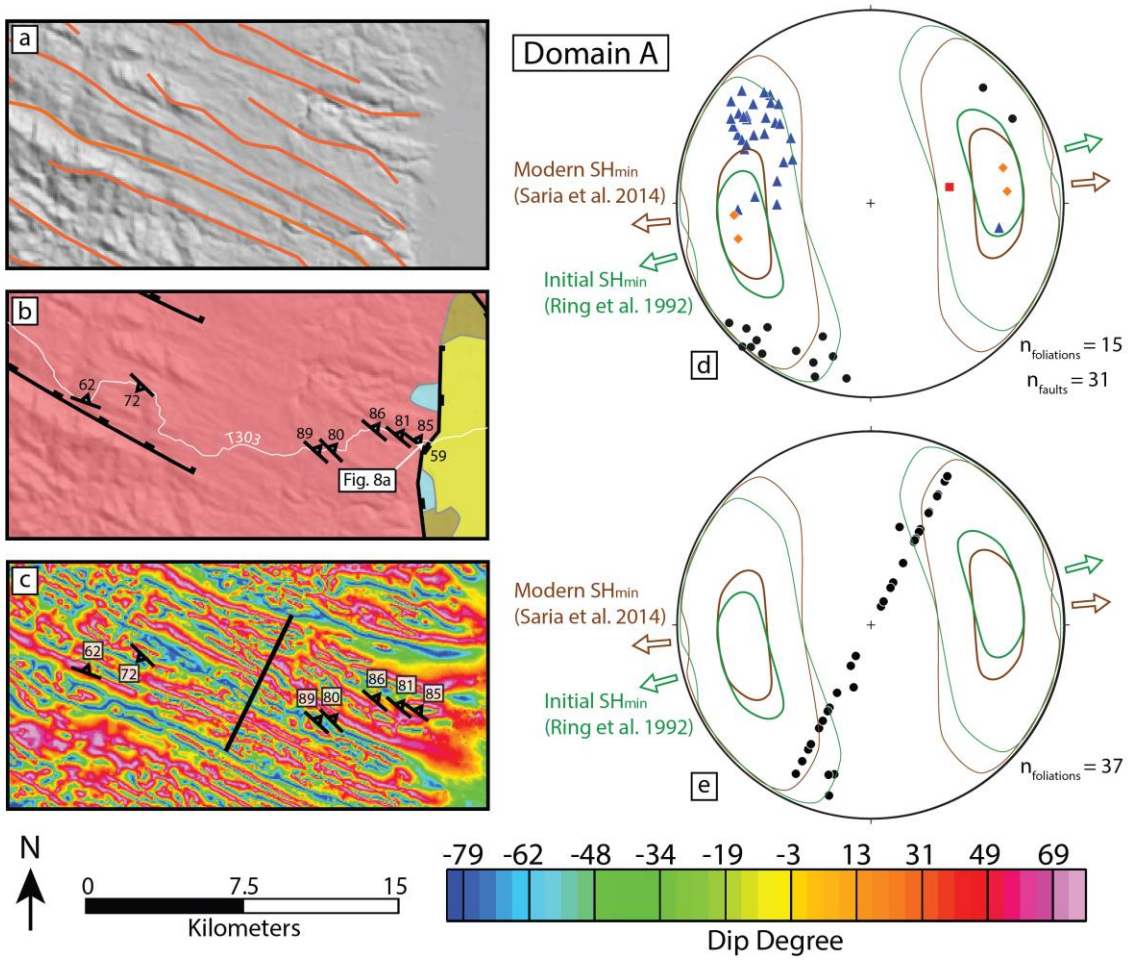


Figure 8. To effectively describe the structure of each domain (Figs. 8, 10–15), we followed a presentation that includes five components: (a) A hillshade SRTM DEM with a 45° sun elevation angle and 45° azimuth. The orange lines represent the structural trajectories of the regional foliation associated with the MSZ. These trends were traced from the total horizontal derivative of the aeromagnetic data (Fig. 5); (b) the geologic map with foliation, bedding, and fault orientation field measurements; (c) the aeromagnetic tilt map with the foliation field measurements overlain. Positive dips (pink, red, and orange colors) indicate east-dipping structures, while negative dips (blue, green, and yellow) indicate west-dipping structures. The long black line shows the transect where we sampled the tilt map every 200 m for dip degrees; (d) lower hemisphere equal area stereographic projections of each domain. Black dots represent poles to foliations, blue triangles represent poles to normal faults, red squares represent striations, and orange diamonds represent the poles to ideal Andersonian normal faults for each stress regime. The smaller green contours show the area of high likelihood of structural fabric reactivation (Morley et al. 2004) for the initial $SH_{min}$ orientation of the Malawi Rift (Ring et al. 1992) and the larger contours show the area of moderate likelihood of reactivation. Brown contours represent the same reactivation chances under the modern $SH_{min}$ direction (Saria et al. 2014); (e) follows the same conditions as described in (d), except the stereonets contain foliation orientations extracted every 200 m along profiles taken from the aeromagnetic tilt map. Each plot shows several poles to foliation planes as having dips from 0° to 40°; since we never observed such shallow dips in the field we believe these are artifacts introduced while calculating the tilt map. Trends of the poles to foliation planes appear abnormally constant due to the difficulty of manually discerning small variations in strike. Domain A best illustrates the strong agreement between foliation planes measured from the aeromagnetic tilt map and those measured in the field. The NW–SE strike of the foliation planes is at a high angle to both the modern and initial extensional directions.

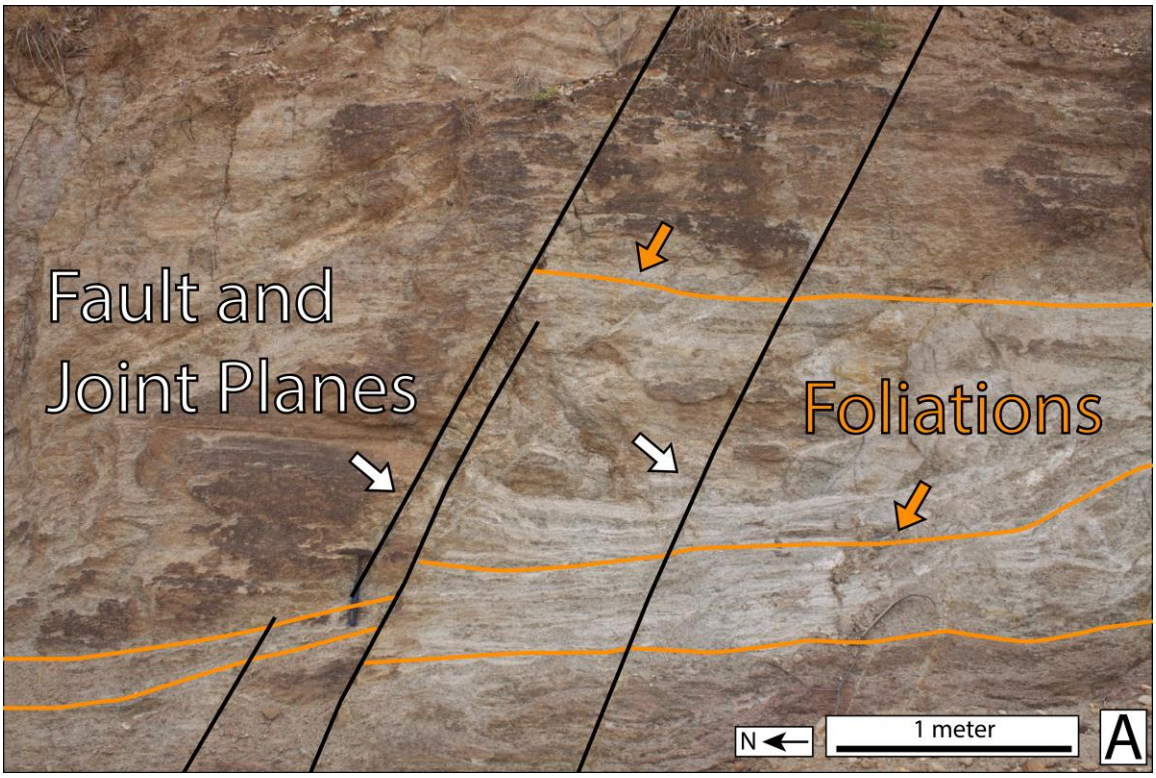
Fault and
Joint Planes
Foliations
N
1 meter
A

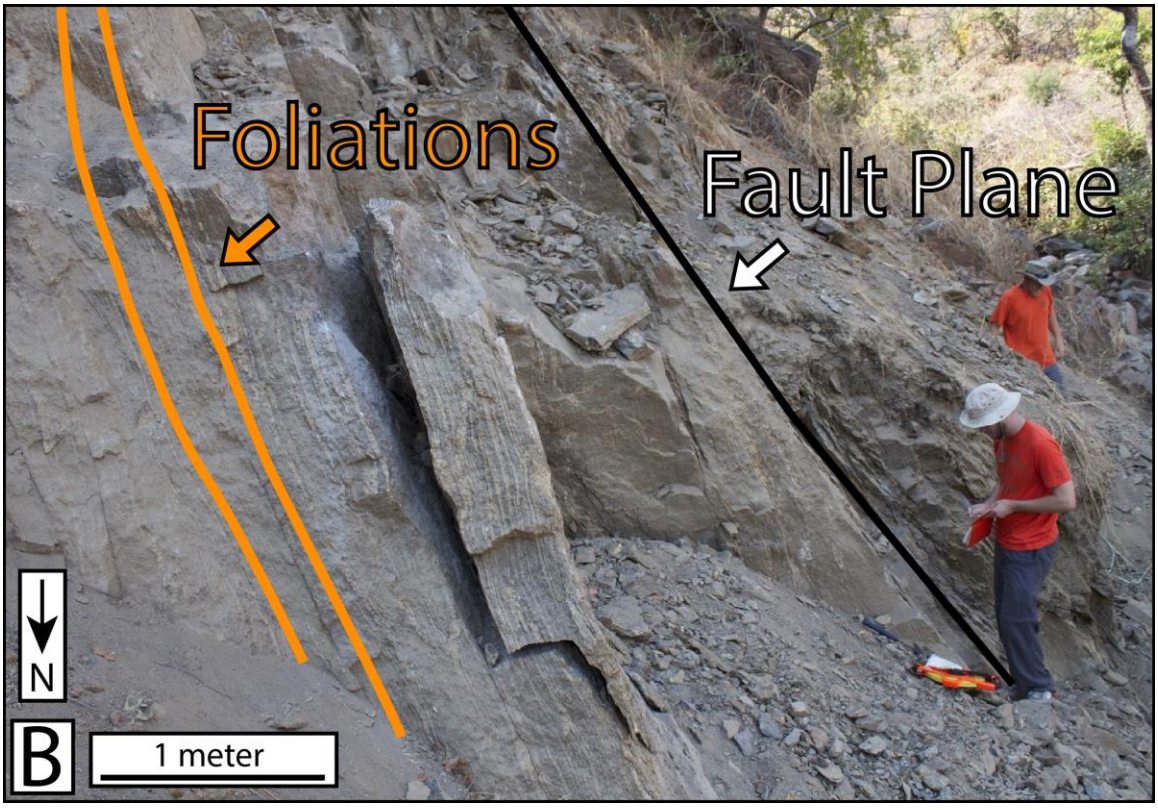
Foliations
Fault Plane
N
B
1 meter


Figure 9. (a) Foliation planes are disrupted by faults in Domain A. The foliations strike NW and are steeply dipping, while the faults strike NE and dip between 40° and 70°. (b) A fault plane and foliations with similar orientations in Domain C. The foliations strike NNW with dips between 70 and 80°. (c) Foliation plane surface exhibiting striations and normal fault stepping from the same fault shown in (b). This fault plane strikes 162° and dips 81° to the west.

aeromagnetic tilt data (Fig. 8c). Both methods of measuring the foliation orientations show the foliation planes clustering near the outer limits of the contours that indicate a moderate likelihood of reactivation (Fig. 8d, e). Tilt values extracted from the aeromagnetic tilt map show a wide range of foliation plane dips, with most values over 45° (Fig. 8e). Fault strikes in this region were nearly perpendicular to the strikes of foliation planes (Fig. 9a).

*Domain B*

Domain B is the domain that is furthest from the fault escarpments along the western flank of the North Basin. This domain has foliation planes with poles to strikes from NNW to NNE and dips primarily between 50° and 80° as measured by both the field data and aeromagnetic tilt data (Fig. 10d, e). In areas where the aeromagnetic tilt did not exhibit a linear magnetic signature, the field measurements regularly deviated 20° or more from the regional strike (Fig 10c). Two of the 13 normal faults in this area had a similar orientation to the foliation planes, but the normal faults did not follow a consistent orientation.

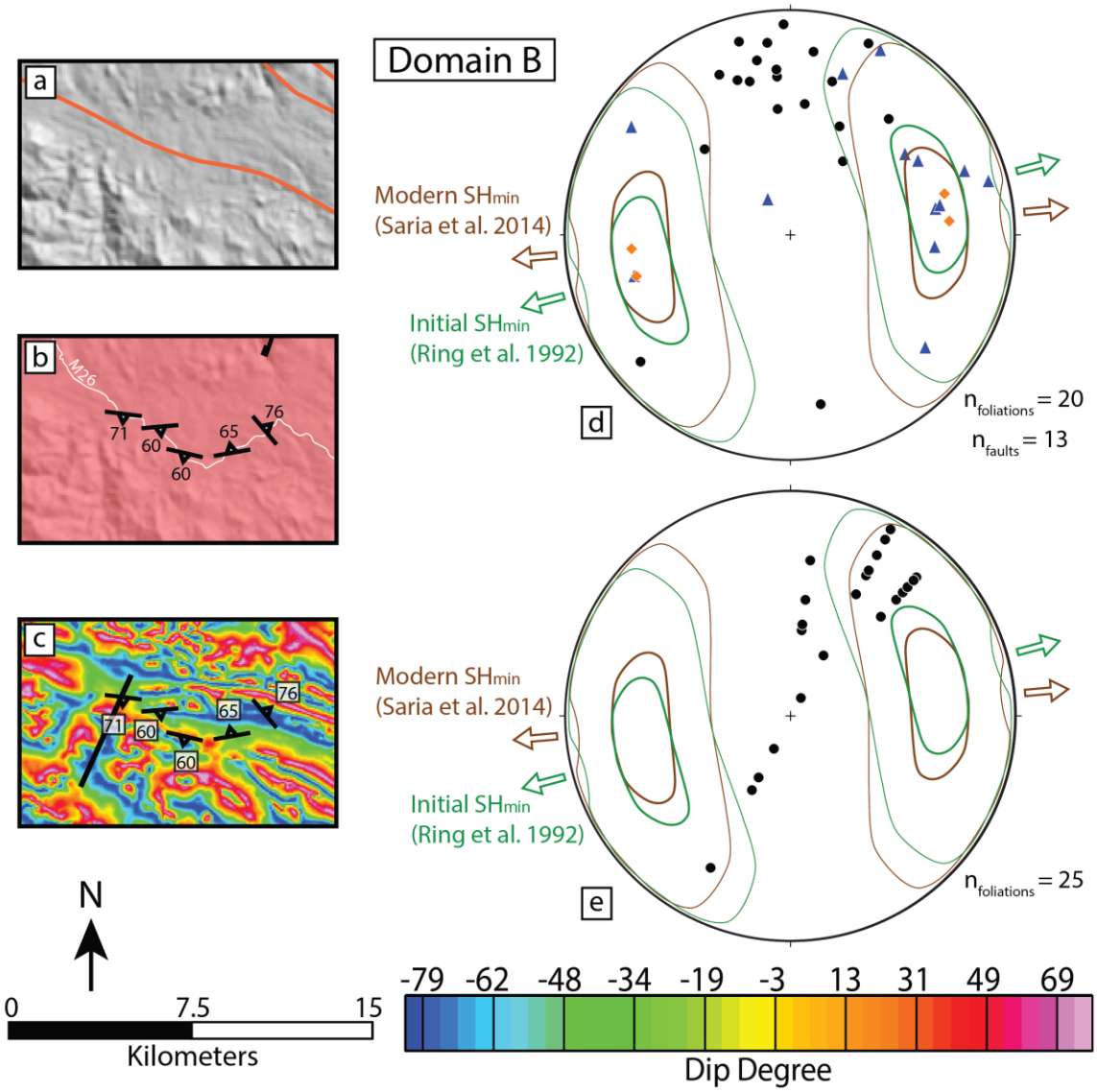


Figure 10. Field measurements and remotely-sensed data for Domain B. Sub-figures (a) through (e) are described in detail in Figure 8. Poles to foliation planes generally trend NNW to NNE in this domain, which is at a high angle to the extensional direction.

*Domain C*

Domain C contains foliations with a regional aeromagnetic strike of 302° in the northwest and a strike of 321° in the southeast, illustrating a macroscopic fold in the middle of the domain. South of this bend we observed the inception of multiple fault escarpments (Fig 11b), contrasting the lone fault escarpment in Domain A. Field measurements of the foliation orientations showed NNE to ENE strikes with dips

typically between 70° and 90° (Fig 11d). The foliation plane field measurements closely matched those of the aeromagnetic tilt map except for at the end of a Karoo horst near the middle of the domain (Fig 11b, c). Two of the foliation planes we measured lie within the contours that indicate a high likelihood of reactivation. The 11 normal faults we measured did not follow a consistent orientation. One of the normal faults slipped along a foliation plane (Fig. 9b) and exhibited stepping along that same plane (Fig. 9c).

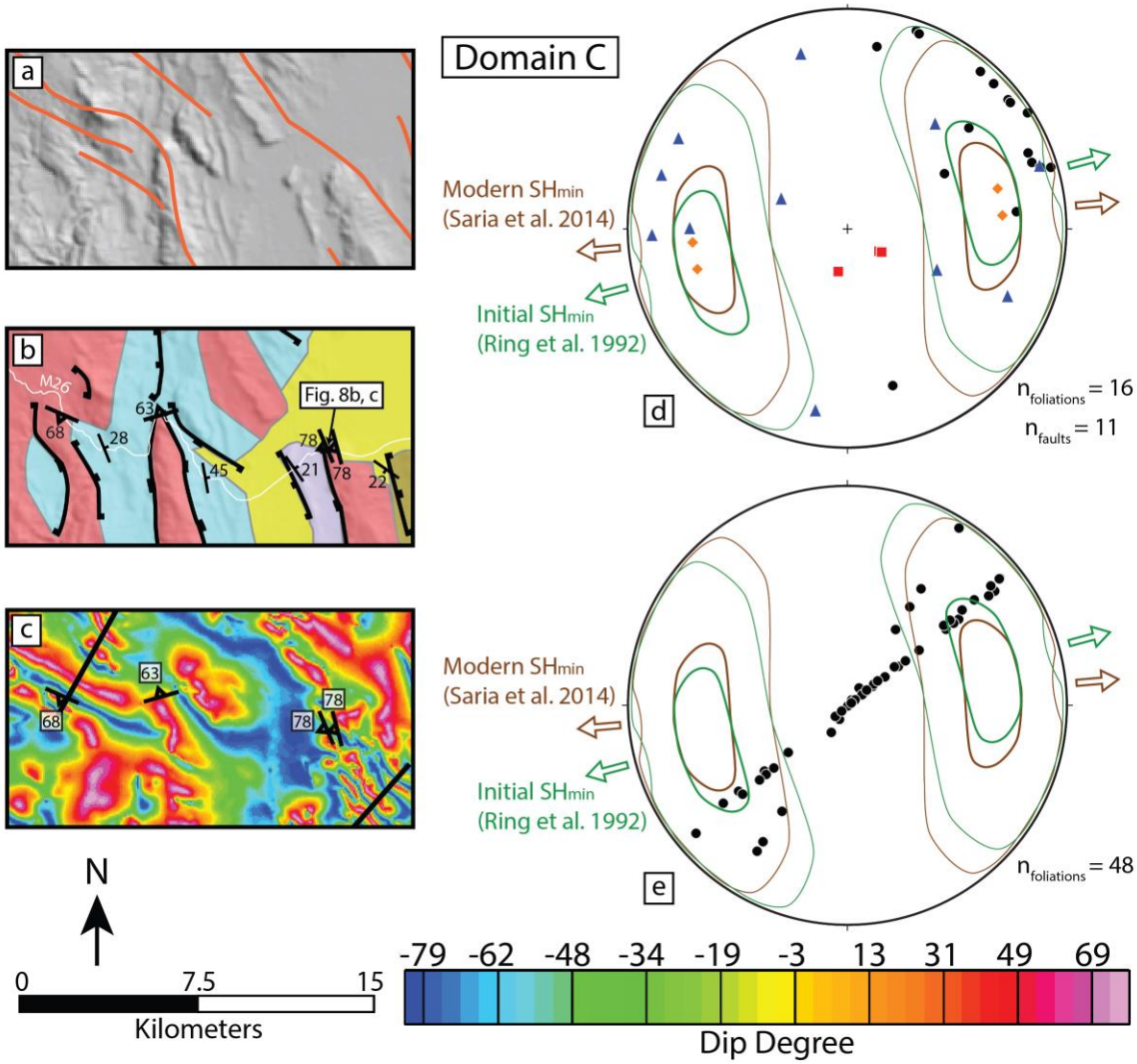


Figure 11. Field measurements and remotely-sensed data for Domain C. Sub-figures (a) through (e) are described in detail in Figure 8. Here the foliation planes in the MSZ show a macroscopic fold as they change from a NW strike to a NNW strike. North of this fold we observed a concentrated deformation zone, and south of the fold we observed a 16 km wide zone of distributed faulting.

*Domain D*

Domain D contains foliations with a regional aeromagnetic strike from 330° in the northwest portion to 349° in the eastern portion (Fig 12c, e). Four of the foliation planes measured in the field lie within the contours that indicate a high likelihood of reactivation (Fig 12d). This domain exhibits a 16 km zone of fault escarpments that are adjacent to Permo-Triassic, Cretaceous, Mio-Pleistocene, and Quaternary sediments (Fig 12b). The 11 measured normal faults in this domain typically lie within the 30° strike difference from the extensional direction needed to be included in the zone of high likelihood of reactivation, but they all lie outside of this zone due to their >70° dips.

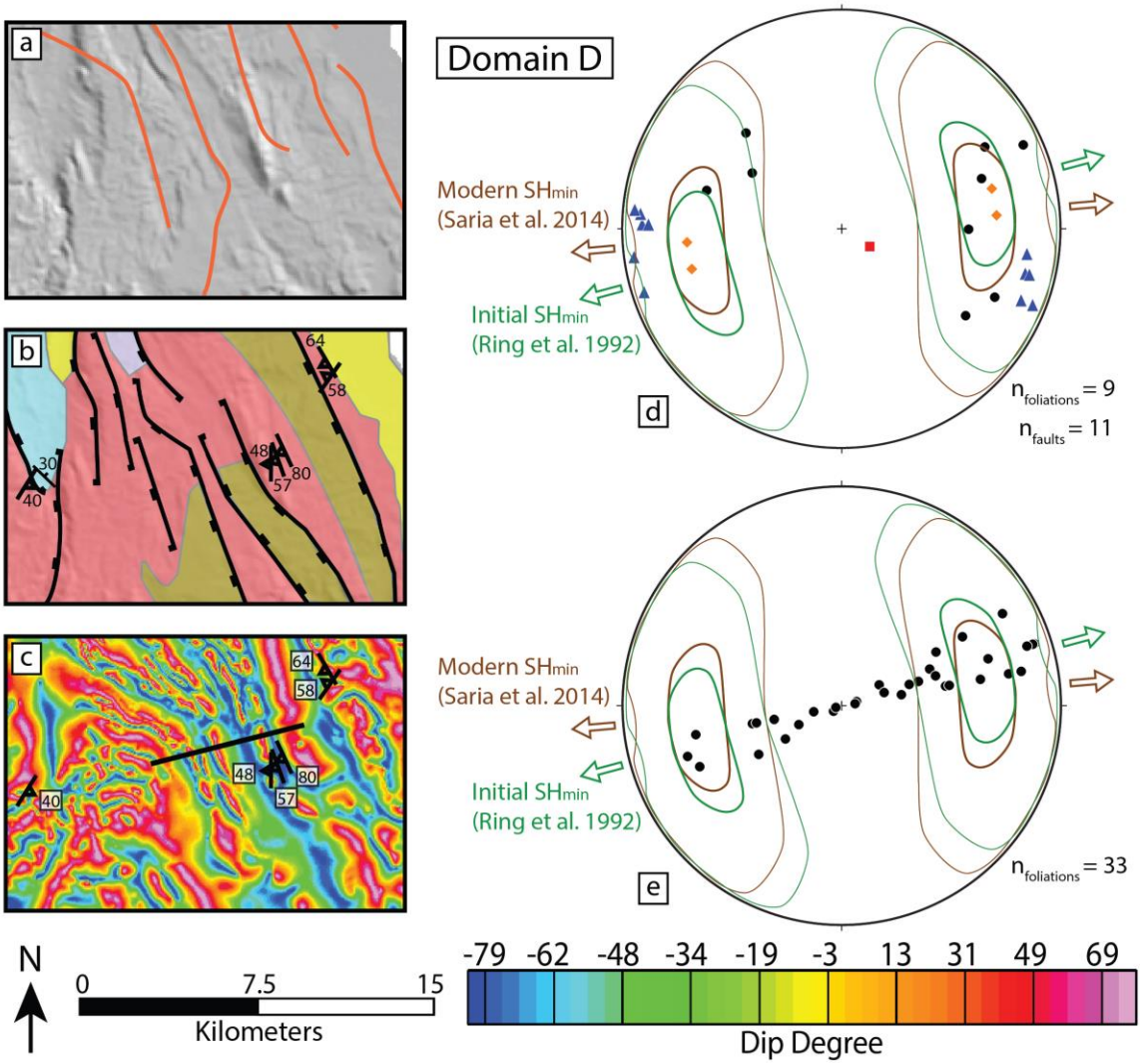


Figure 12. Field measurements and remotely-sensed data for Domain D. Sub-figures (a) through (e) are described in detail in Figure 8. This domain illustrates the wide zone of deformation when the poles to the foliation planes measured in the field and measured from the aeromagnetic data align with the extensional direction. Note the mesoscopic-scale fold in the middle-right of the geologic map shown in (b).

*Domain E*

The regional aeromagnetic strike of foliations within Domain E was between 326° and 337°. Several poles to the aeromagnetic foliation planes lie within the contours that indicate a high likelihood of reactivation (Fig. 13e). The field measurements support the regional aeromagnetic strike, and the foliation planes we observed in the field have poles that typically plot within 10° strike or 10° dip of the contours that represent a high

likelihood of reactivation (Fig. 13d). The two fault planes we were able to measure in the southeast portion of the domain support the strike of the mapped escarpment (Fig. 13b).

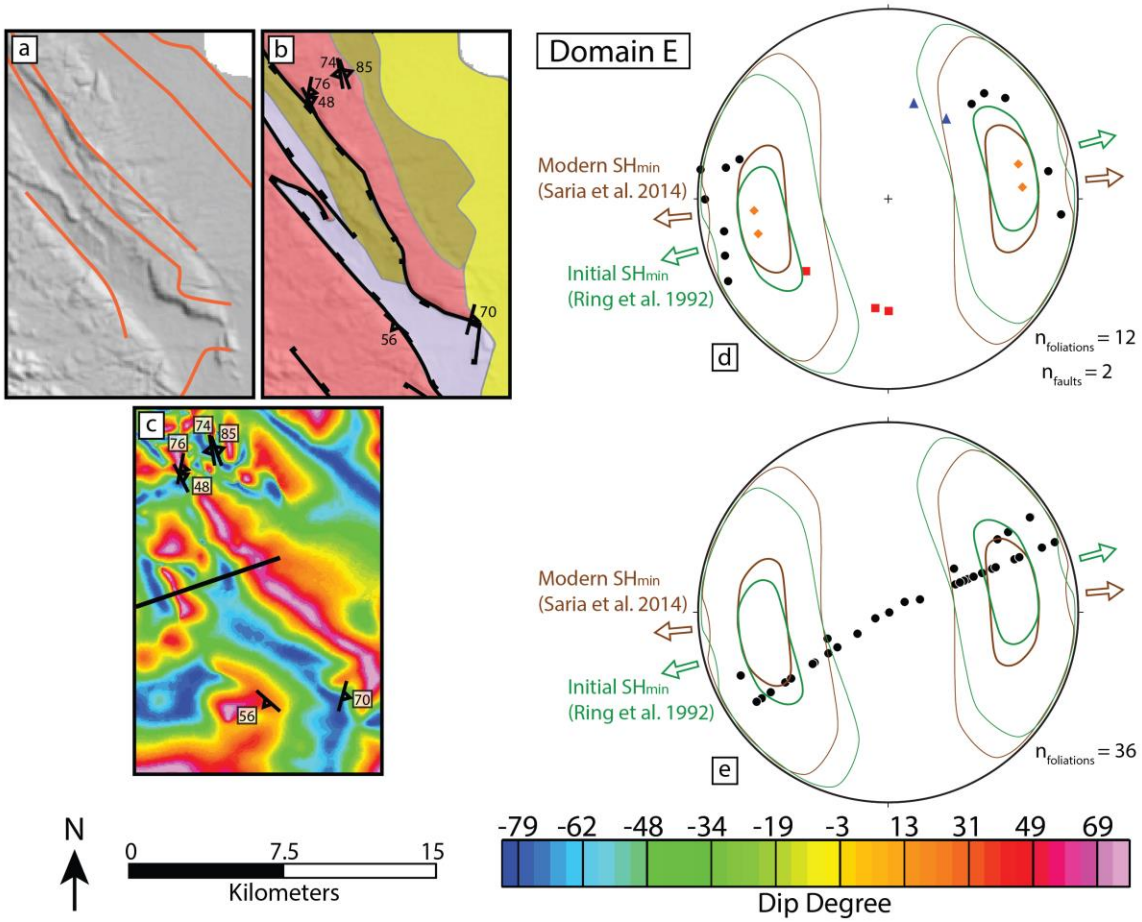


Figure 13. Field measurements and remotely-sensed data for Domain E. Sub-figures (a) through (e) are described in detail in Figure 8. In this domain the poles to foliation planes measured in the field and from the aeromagnetic data align with the extensional direction, similar to Domain D.

*Domain F*

Domain F contains the southernmost extent of the MSZ in our study area. This domain has two perpendicular aeromagnetic foliation strikes of 218° and 308° (Fig. 14e). One of the foliation planes we were able to measure in the field plots within the contour representing a high likelihood of reactivation, though there is insufficient data to draw many conclusions from this domain (Fig. 14d). The single fault escarpment in this

domain changes strike from NNW to NW, and our field measurements show normal fault orientations striking N-S to E-W.

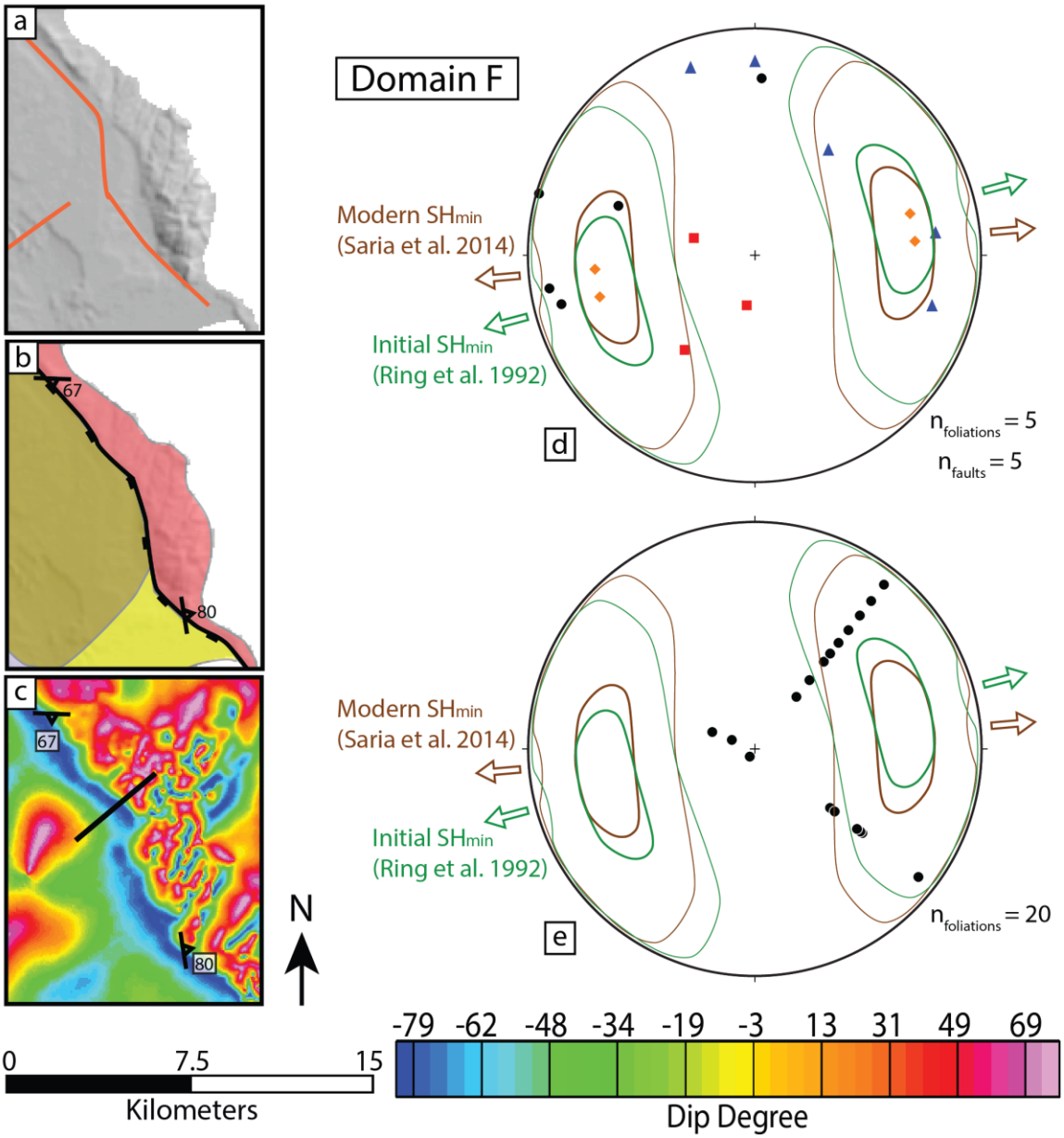


Figure 14. Field measurements and remotely-sensed data for Domain F. Sub-figures (a) through (e) are described in detail in Figure 8. The aeromagnetic data shows there are two perpendicular trends for the poles to foliation planes in this area.

*Domain G*

Domain G is the only area we sampled that did not contain foliations that formed in the MSZ. Aeromagnetic foliations showed a 254° strike (Fig. 15c, e) and our few field

measurements showed foliation strikes from ENE to NW. Four of the normal faults we measured in this domain exhibited an E-W strike while one normal fault slipped along a foliation plane striking N-S (Fig. 15d). There is a lone fault escarpment in this domain that strikes NNW to NW.

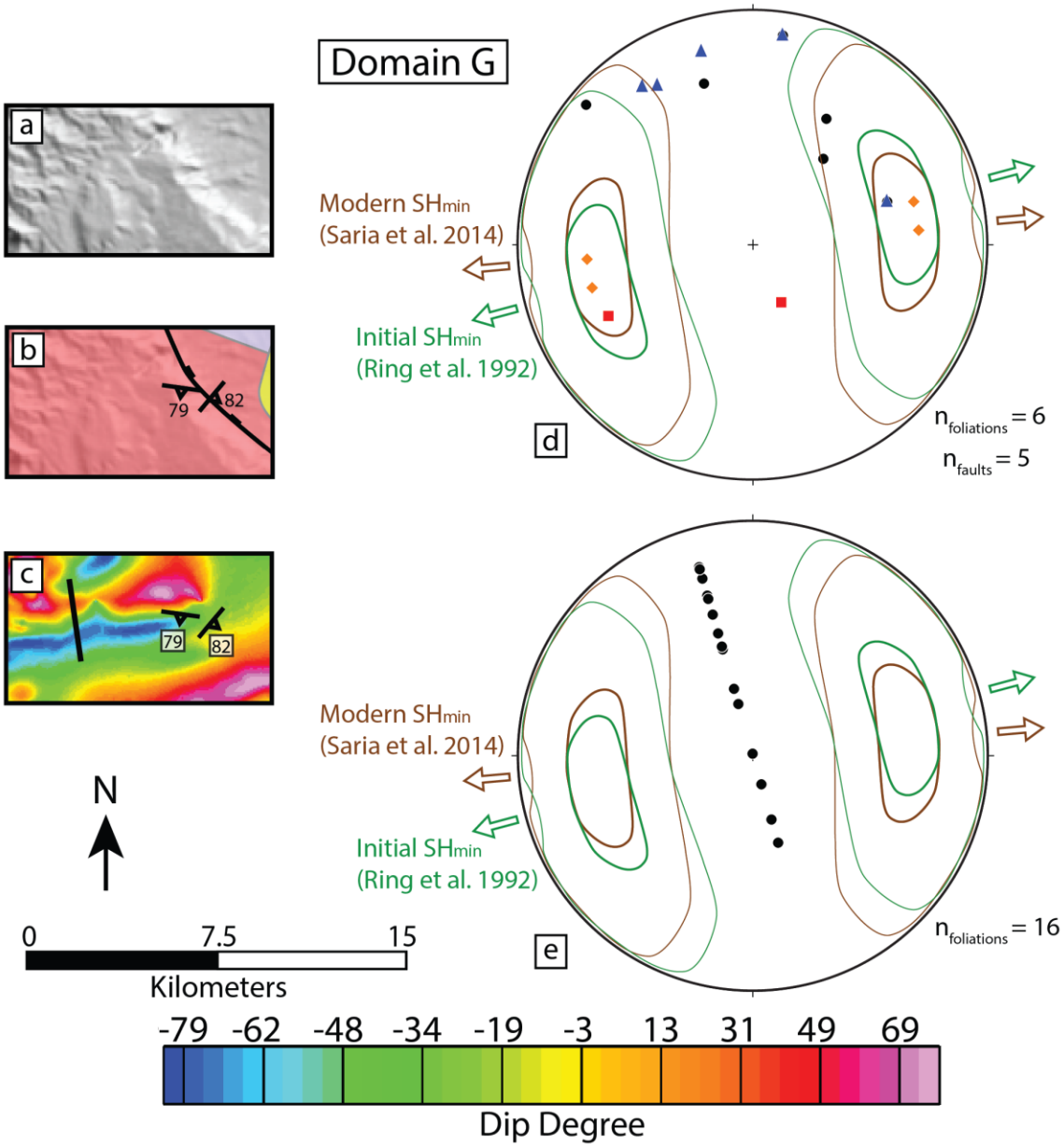


Figure 15. Field measurements and remotely-sensed data for Domain G. Sub-figures (a) through (e) are described in detail in Figure 8. This domain is outside the MSZ. The poles to the foliation planes are typically at a high angle to the extensional direction.

*Fault Characteristics from Remote Sensing*

SRTM DEM hillshade maps revealed four 30–50 km long escarpments, six 15–30 km long escarpments, and at least 25 2–15 km long escarpments striking NNW within 70 km southwest of the Livingstone border fault on its exposed hanging wall west of the lake (Fig. 3). We delineated several faults that both serve as bounding faults formed during the Jurassic Karoo Rift System (Fig. 3).

Faults distribution changes along the Karonga Fault Zone. Cross-section W-W' (Fig. 3a, b) shows the ~20 km long fault in the basement rock in the northernmost part of our study area. Further south along cross-sections X-X' and Y-Y', this area contains several faults, horsts, and grabens instead of one fault as seen in W-W'. Permo-Triassic, Cretaceous, and Mio-Pleistocene sediments along these faults show they have been active since the late Paleozoic (Fig. 3a). Cross-section Z-Z' shows the southernmost portion of the Karonga Fault Zone contains one fault as opposed to the multiple faults bounding the horsts and grabens seen in X-X' and Y-Y'.

*Aeromagnetic Data*

The filters applied to the aeromagnetic data showed the Precambrian foliation of the basement rocks, including those from the MSZ. Figure 5 shows the filtered data and lineations traced from the aeromagnetic data. Around 9° 55' S, the latitude of Karonga, we saw a shift in Domain C from the foliation planes striking from 302° in the northwest portion of the domain to 321° in the southeast portion. The foliations from the MSZ are last exposed in this area in Domain F, where the planes strike 218° and 308° (Fig. 14e). Domain G did not contain any lineations from the MSZ.

# CHAPTER V

# DISCUSSION & CONCLUSIONS

## *Interpreting Basement Fabric through Aeromagnetic Data*

The foliation orientations from aeromagnetic data have been confirmed by field measurements in several domains, which gives us confidence that the map is valid outside the locations measured in the field. Domain A is the best example of this agreement, as shown by the matching strike of the traced lineations and the corresponding poles to foliation planes in Figure 8. Stereonets of foliations mapped from the aeromagnetic data illustrate the natural variation of dip angles of foliation planes that are created during the formation of shear zones such as the MSZ. These plots highlight the linear trends of the aeromagnetic data that represent the regional strike for foliations within each domain.

The wide range of dips we observed in the field is evidence that the rapid changes in dip seen in the aeromagnetic tilt map are possible. Though we measured variations of the strike of the foliations within each domain in the field, the general trends seen in the aeromagnetic data indicate that these are small folds that cluster around a regional strike that could potentially accommodate slip. Previous maps (Ring, 1994) could only sample small portions of the basement fabric where outcrops were exposed

and accessible, while the maps presented in this study are able to image the fabric throughout the entire western flank of the North Basin of the Malawi Rift.

*Strain Accommodation*

If foliations are dipping 50–70° and within 30° strike of the minimum horizontal stress direction, these are considered to be favorable conditions for slip along those weak planes in an extensional stress regime (Morley 2004). There is a moderate likelihood that foliations within 60° strike and dipping 40°–90° would slip as well. On a stereographic projection, the closer that poles to foliations plot to the ideal Andersonian normal fault, the likelier the foliations are to be suitably oriented for slip. We will be able to interpret the effect of the structural fabric on normal fault plane orientations by analyzing their changes between structural domains.

In the northern portion of the rift where the foliations strike NW (Fig. 8), the NNE-striking escarpment does not follow the strike of the foliations and is not slipping along these structures. However, Karoo growth strata suggest that this fault initially broke in the Permo-Triassic and could have reactivated once the Malawi Rift began to form (Fig. 3).

The pre-existing structures in Domain B have likely not reactivated to accommodate strain due to the regional NNW to NNE poles to foliation planes. These poles are at too high of an angle to the direction of extension to fall within the contours that indicate a high likelihood of reactivation (Fig. 10d, e), and the lack of major escarpments in this area suggests not much strain is accommodated in this domain (Fig. 10b).

Where the strike of the foliations bend from NW to NNW near 9° 55’ S in Domain C, the faults follow a similar strike to the foliations but have varying dips (Fig. 11). This corresponds to a change from a single escarpment north of Karonga to the area of distributed faulting in the south. Cross-sections in Figure 3 taken across the length of the Karonga fault zone highlight this abrupt change. Following Morley et al. (2004), several of these poles to faults and foliations are within the 30° trend and 10° plunge orientation difference from an Andersonian normal fault, showing the faults could lie along foliation planes of weakness. The dip of the foliations changes quickly over a short distance in some places (Figs. 12, 13), suggesting that fault planes could have formed where the dip of the foliations was favorable for slip. The aeromagnetic data (Fig. 5) shows that the foliations broadly follow the same strike for long distances even though there are local variations.

Rather than one dominant escarpment, several faults longer than 30 km accommodate the strain in Domains C through F. Areas with foliations close to perpendicular to the initial or modern minimum stress direction were likely able to slip along the foliation planes. The sediments bounded by some of these ridges show that these faults were active during previous rifting events, suggesting that these faults planes previously slipped along the foliation planes and now the old rift-related faults are being reactivated. Whether the stress regime from the Malawi Rift or a previous regime created these faults, it seems likely that they slipped along the foliation planes.

This result conflicts with the result of Ring (1994), which stated that the foliations and faults did not share a similar geometric relationship. However, the empirical observations of fault and foliation orientations, and the general strike of the foliations

combined with its range of dips shows that the foliations from Domains C though F have slip along these planes. This style of strain accommodation is illustrated in Figure 16. We propose that the Karonga Fault System lies at the fold axis of the rollover anticline in the hanging wall of the Livingstone Border Fault. Models of hanging wall deformation in listric fault systems (e.g. McClay and Ellis 1987, Withjack et al. 1995) suggest that the majority of extensional stress is accommodated above the listric fault plane and adjacent to where the listric fault plane becomes horizontal. However, Withjack et al. (1995) shows that the fold axis of the rollover anticline also accommodates strain regardless of the listric fault geometry. Thus, the weak foliated planes of the MSZ are likely to have accommodated strain as the Livingstone Border Fault hanging wall was deforming. The modern seismicity suggests that extension is still being accommodated in the Karonga Fault Zone (Fig. 4).

South of Domain F, the MSZ disappears underneath the Malawi Lake and the Karonga Fault Zone resumes its surface expression as a single escarpment as shown in

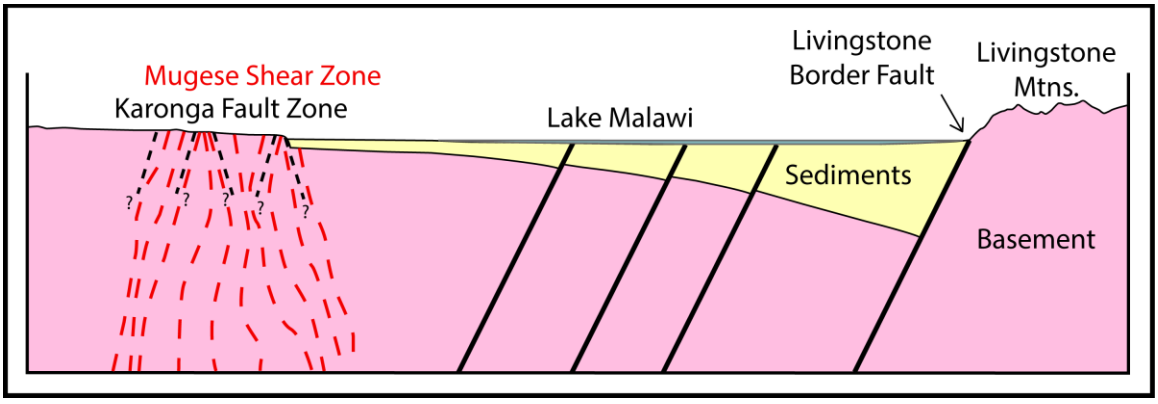


Figure 16. Schematic cross-section of the Livingstone Border Fault hanging wall deformation within Domains C, D, E, and F. Depths of faults within the Karonga Fault Zone are unknown. We suspect that the Karonga Fault Zone is the result of deformation along the fold axis of the rollover anticline in the hanging wall of the Livingstone border fault. Where weak foliation planes of the Mugese Shear Zone are suitably oriented to the maximum extensional direction, faults likely developed along those planes. Modified from Biggs et al. (2010).

Domain G. Here the basement rock is foliated and strikes in various orientations that doesn't follow a consistent direction that could localize strain.

*Implications for Seismic Hazard*

Earthquake epicenters since 1901 show that most active deformation in this area is concentrated in the zone of distributed faulting, primarily in Domains C and D. Epicenters of the 2009 earthquake swarm occurred in this same area, as well as further to the north (Fig. 4).

The concentration of seismic activity where the foliations align with faults (Fig. 4) shows that regions with a dominant strike of foliations near-perpendicular to the modern $SH_{min}$ are at risk for earthquakes. The fault escarpment from the 2009 earthquake sequence (Machayeki et al. 2015) lies directly on an area with foliations that are favorably oriented for slip. We hypothesize that future earthquakes will occur along new or reactivated fault planes that parallel the foliation lineations mapped in Figure 5.

The 2.2 mm/yr modeled rift opening velocity (Saria et al. 2014) implies that this area will see future seismic activity. Since the Livingstone border fault has likely reached its maximum displacement (Scholz and Contreras 1998), most strain accommodation has likely migrated to the hanging wall. The pre-existing foliations and faults here will likely serve as effective weak planes for future deformation in response to the divergence.

*Conclusions*

In this paper, we presented the results of aeromagnetic, remote sensing, and meso-scale structural data analysis of the Karonga Fault Zone and the MSZ to characterize

strain localization of the greater Karonga area. The results of this study suggest that portions of the bounding faults along the western flank of the North Basin of the Malawi Rift are slipping along basement foliations from the MSZ and faults from previous rifting events. In areas where the foliations strike close to perpendicular to the modern or historic $SH_{min}$, there has likely been slip along the foliation planes. In such areas, we see a wide zone of deformation that consists of several faults longer than 30 km that accommodate the extension. The regional strike of foliations measured from the aeromagnetic data shows that the meso-scale folds reported in Ring (1994) do not interfere with the general ability of the foliation planes to localize and accommodate strain in some areas (Domains C through F). Where the foliations are not preferably aligned with regard to $SH_{min}$, one fault accommodates the strain in that area. These faults formed from previous rifting regimes, which have been reactivated. Regional foliation trends are at risk of slipping, creating a seismic hazard where the MSZ foliation is favorably oriented in the hanging-wall of the Livingstone border fault.

# REFERENCES

Allmendinger, R. W., Cardozo, N. C., & Fisher, D., 2012, Structural Geology Algorithms: Vectors & Tensors: Cambridge, England, Cambridge University Press, 289 pp.

Anderson, E. M. (1951). The dynamics of faulting and dyke formation with applications to Britain. Hafner Pub. Co..

Biggs, J., Nissen, E., Craig, T., Jackson, J., & Robinson, D. P. (2010). Breaking up the hanging wall of a rift-border fault: The 2009 Karonga earthquakes, Malawi. *Geophysical Research Letters*, *37*(11).

Buck, W. R. (2006). The role of magma in the development of the Afro-Arabian Rift System. *Geological Society, London, Special Publications*, *259*(1), 43-54.

Chorowicz, J. (2005). The East African Rift System. *Journal of African Earth Sciences*, *43*(1), 379-410.

Cloos, E. (1968). Experimental analysis of Gulf Coast fracture patterns. *Aapg Bulletin*, *52*(3), 420-444.

Coulomb, C.A. (1776). Sur une application des maximis et minimis a quelques problems de statique, relatives a l'architecture. Acad Sci Paris Mem Math Phys 7:343–382.

Coussement, C., Gente, P., Rolet, J., Tiercelin, J. J., Wafula, M., & Buku, S. (1994). The North Tanganyika hydrothermal fields, East African Rift system: their tectonic control and relationship to volcanism and rift segmentation. *Tectonophysics*, *237*(3), 155-173.

Daly, M. C., Chorowicz, J., & Fairhead, J. D. (1989). Rift basin evolution in Africa: the influence of reactivated steep basement shear zones. *Geological Society, London, Special Publications*, *44*(1), 309-334.

Delvaux, D. (2001). Karoo rifting in western Tanzania: Precursor of Gondwana breakup. *Contributions to geology and paleontology of Gondwana in honor of Helmut Wopfner: Cologne, Geological Institute, University of Cologne*, 111-125.

Dhaoui, M., Gabtni, H., Jallouli, C., Jleilia, A., Mickus, K., & Turki, M., (2014). Gravity analysis of the Precambrian basement topography associated with the northern boundary of Ghadames Basin (southern Tunisia), *J. Appl. Geophysics, 111*, p. 299-311.

Doblas, M. (1998). Slickenside kinematic indicators. *Tectonophysics*, *295*(1), 187-197.

Geological Survey of Malawi (1966), Geological map of Malawi, scale 1/1,000,000, Geol. Surv. of Malawi, Lilongwe.

Espurt, N., Callot, J. P., Roure, F., Totterdell, J. M., Struckmeyer, H. I., & Vially, R. (2012). Transition from symmetry to asymmetry during continental rifting: an example from the Bight Basin–Terre Adélie (Australian and Antarctic conjugate margins). *Terra Nova*, *24*(3), 167-180.

Fairhead, J. D., Salem, A., Cascone, L., Hammill, M., Masterton, S., & Samson, E. (2011). New developments of the magnetic tilt-depth method to improve structural mapping of sedimentary basins. *Geophysical Prospecting*,*59*(6), 1072-1086.

Fritz, H., Abdelsalam, M., Ali, K. A., Bingen, B., Collins, A. S., Fowler, A. R., ... & Macey, P. (2013). Orogen styles in the East African Orogen: a review of the Neoproterozoic to Cambrian tectonic evolution. *Journal of African Earth Sciences*, *86*, 65-106.

Katumwehe, A. B., Abdelsalam, M. G., & Atekwana, E. A. (2015a). The role of pre-existing Precambrian structures in rift evolution: The Albertine and Rhino grabens, Uganda. *Tectonophysics*, *646*, 117-129.

Katumwehe, A. B., Abdelsalam, M. G., Atekwana, E. A., & Laó-Dávila, D. A. (2015b). Extent, kinematics and tectonic origin of the Precambrian Aswa Shear Zone in eastern Africa. *Gondwana Research*.

Keranen, K., & Klemperer, S. L. (2008). Discontinuous and diachronous evolution of the Main Ethiopian Rift: Implications for development of continental rifts. *Earth and Planetary Science Letters, 265*(1), 96-111.

Korme, T., Acocella, V., & Abebe, B. (2004). The role of pre-existing structures in the origin, propagation and architecture of faults in the Main Ethiopian Rift. *Gondwana Research*, *7*(2), 467-479.

Laó-Dávila, D. A., Al-Salmi, H. S., Abdelsalam, M. G., & Atekwana, E. A. (2015). Hierarchical segmentation of the Malawi Rift: The influence of inherited lithospheric heterogeneity and kinematics in the evolution of continental rifts. *Tectonics*, *34*(12), 2399-2417.

Macheyeki, A. S., Mdala, H., Chapola, L. S., Manhiça, V. J., Chisambi, J., Feitio, P., ... & Goitom, B. (2015). Active fault mapping in Karonga-Malawi after the December 19, 2009 Ms 6.2 seismic event. *Journal of African Earth Sciences*, *102*, 233-246.

Marrett, R., & Allmendinger, R. W. (1990). Kinematic analysis of fault-slip data. *Journal of Structural Geology*, *12*(8), 973-986.

McClay, K. R., & Ellis, P. G. (1987). Geometries of extensional fault systems developed in model experiments. *Geology*, *15*(4), 341-344.

McConnell, R. (1972). Geological development of the rift system of East Africa. *Geol. Soc. Am. Bull.*, *83*, 2549–2572.

Mohr, O. (1900). Welche Umstände bedingen die Elastizitätsgrenze und den Bruch eines Materials? Zeit des Ver Deut Ing 44:1524–1530.

Morley, C. K., Haranya, C., Phoosongsee, W., Pongwapee, S., Kornsawan, A., & Wonganan, N. (2004). Activation of rift oblique and rift parallel pre-existing fabrics during extension and their effect on deformation style: examples from the rifts of Thailand. *Journal of Structural Geology*, *26*(10), 1803-1829.

Morley, C. K. (2010). Stress re-orientation along zones of weak fabrics in rifts: An explanation for pure extension in 'oblique'rift segments?. *Earth and Planetary Science Letters*, *297*(3), 667-673.

Mortimer, E., Paton, D. A., Scholz, C. A., Strecker, M. R., & Blisniuk, P. (2007). Orthogonal to oblique rifting: effect of rift basin orientation in the evolution of the North basin, Malawi Rift, East Africa. *Basin Research*, *19*(3), 393-407.

Ring, U., Betzler, C., & Delvaux, D. (1992). Normal vs. strike-slip faulting during rift development in East Africa: the Malawi rift. *Geology*, *20*(11), 1015-1018.

Ring, U. (1994). The influence of preexisting structure on the evolution of the Cenozoic Malawi rift (East African rift system). *Tectonics*, *13*(2), 313-326.

Ring, U., Kröner, A., Buchwaldt, R., Toulkeridis, T., & Layer, P. W. (2002). Shear-zone patterns and eclogite-facies metamorphism in the Mozambique belt of northern Malawi, east-central Africa: implications for the assembly of Gondwana. *Precambrian Research*, *116*(1), 19-56.

Saria, E., Calais, E., Stamps, D. S., Delvaux, D., & Hartnady, C. J. H. (2014). Present-day kinematics of the East African Rift. *Journal of Geophysical Research: Solid Earth*, *119*(4), 3584-3600.

Scholz, C.H., & Contreras, J. C. (1998). Mechanics of continental rift architecture. *Geology*, *26*(11), 967-970.

Sperner, B., & Zweigel, P. (2010). A plea for more caution in fault–slip analysis. *Tectonophysics*, *482*(1), 29-41.

Tingay, M. R., Morley, C. K., Hillis, R. R., & Meyer, J. (2010). Present-day stress orientation in Thailand's basins. *Journal of Structural Geology*, *32*(2), 235-248.

United States Geological Survey (2016). Earthquake Archives, accessed Oct. 10, 2015. <http://earthquake.usgs.gov/earthquakes/search/>.

Withjack, M. O., Islam, Q. T., & La Pointe, P. R. (1995). Normal faults and their hanging-wall deformation: an experimental study. *AAPG bulletin*, *79*(1), 1-17.

# APPENDICES

## APPENDIX A

1) Table of Foliation Orientations

| Domain | Latitude | Longitude | Strike (°) | Dip (°; RHR) |
|---|---|---|---|---|
| A | 9° 45.343' S | 33° 39.798' E | 290 | 62 |
| | 9° 45.017' S | 33° 41.286' E | 149 | 74 |
| | | | 134 | 72 |
| | | | 310 | 72 |
| | 9° 46.745' S | 33° 46.150' E | 312 | 89 |
| | | | 320 | 85 |
| | 9° 46.674' S | 33° 46.550' E | 315 | 80 |
| | 9° 46.128' S | 33° 47.727' E | 310 | 86 |
| | 9° 46.280' S | 33° 48.371' E | 310 | 81 |
| | | | 278 | 80 |
| | 9° 46.378' S | 33° 48.764' E | 306 | 85 |
| | | | 297 | 74 |
| | 9° 46.452' S | 33° 49.063' E | 284 | 70 |
| | 9° 46.453' S | 33° 49.106' E | 288 | 83 |
| | | | 290 | 76 |
| B | 9° 53.530' S | 33° 33.476' E | 125 | 33 |
| | 9° 53.504' S | 33° 33.459' E | 114 | 44 |
| | | | 88 | 83 |
| | 9° 53.619' S | 33° 33.731' E | 97 | 71 |
| | 9° 53.654' S | 33° 33.880' E | 75 | 78 |
| | 9° 53.626' S | 33° 33.840' E | 84 | 47 |
| | 9° 53.847' S | 33° 34.238' E | 85 | 60 |
| | 9° 53.832' S | 33° 34.127' E | 83 | 75 |
| | 9° 53.939' S | 33° 34.398' E | 71 | 62 |
| | 9° 53.903' S | 33° 34.357' E | 66 | 67 |
| | 9° 54.024' S | 33° 34.498' E | 79 | 68 |
| | 9° 54.072' S | 33° 34.553' E | 75 | 60 |
| | | | 45 | 45 |

| | | | | |
|---|---|---|---|---|
| | 9° 54.359' S | 33° 34.826' E | 105 | 60 |
| | 9° 54.391' S | 33° 34.869' E | 96 | 49 |
| | 9° 54.450' S | 33° 34.956' E | 85 | 63 |
| | 9° 54.265' S | 33° 35.854' E | 260 | 65 |
| | 9° 53.816' S | 33° 36.558' E | 320 | 76 |
| | 9° 53.776' S | 33° 36.635' E | 130 | 57 |
| | | | 112 | 81 |
| C | 9° 56.730' S | 33° 50.579' E | 147 | 87 |
| | 9° 56.680' S | 33° 50.661' E | 141 | 83 |
| | | | 130 | 83 |
| | | | 157 | 78 |
| | | | 142 | 83 |
| | | | 163 | 86 |
| | 9° 56.508' S | 33° 50.838' E | 109 | 85 |
| | | | 110 | 84 |
| | | | 135 | 83 |
| | 9° 56.498' S | 33° 51.036' E | 160 | 78 |
| | 9° 56.588' S | 33° 51.086' E | 135 | 72 |
| | | | 143 | 55 |
| | 9° 56.757' S | 33° 51.204' E | 150 | 42 |
| | 9° 57.332' S | 33° 51.998' E | 140 | 61 |
| | | | 174 | 66 |
| | 9° 55.575' S | 33° 44.261' E | 307 | 69 |
| | | | 308 | 75 |
| | | | 113 | 80 |
| | 9° 55.766' S | 33° 44.292' E | 116 | 83 |
| | 9° 35.722' S | 33° 44.274' E | 125 | 70 |
| | 9° 56.037' S | 33° 44.545' E | 244 | 53 |
| | | | 114 | 68 |
| | | | 249 | 62 |
| | 9° 55.911' S | 33° 46.904' E | 254 | 63 |
| | | | 99 | 73 |
| D | 10° 0.888' S | 33° 55.968' E | 150 | 64 |
| | 10° 3.130' S | 33° 54.540' E | 180 | 48 |
| | 10° 3.063' S | 33° 54.746' E | 160 | 57 |
| | 10° 2.882' S | 33° 54.834' E | 155 | 80 |
| | 10° 1.298' S | 33° 55.922' E | 215 | 58 |
| | | | 204 | 65 |
| | 10° 3.845' S | 33° 49.167' E | 45 | 52 |
| | | | 32 | 40 |

| | | | | |
|---|---|---|---|---|
| | | | 16 | 54 |
| E | 10° 18.397' S | 34° 2.193' E | 131 | 56 |
| | | | 132 | 64 |
| | 10° 18.474' S | 34° 2.280' E | 139 | 70 |
| | 10° 18.376' S | 34° 4.343' E | 15 | 70 |
| | 10° 11.618' S | 34° 0.478' E | 341 | 80 |
| | | | 0 | 86 |
| | | | 349 | 77 |
| | | | 9 | 90 |
| | | | 185 | 80 |
| | 10° 11.642' S | 34° 0.309' E | 170 | 74 |
| | 10° 12.173' S | 33° 59.904' E | 11 | 76 |
| | 10° 12.234' S | 33° 59.900' E | 333 | 84 |
| F | 10° 25.673' S | 34° 14.661' E | 20 | 54 |
| | | | 351 | 81 |
| | | | 346 | 77 |
| | | | 16 | 89 |
| | 10° 20.482' S | 34° 11.444' E | 92 | 67 |
| G | 10° 35.669' S | 34° 8.768' E | 40 | 82 |
| | 10° 35.700' S | 34° 8.673' E | 98 | 79 |
| | | | 162 | 50 |
| | 10° 35.565' S | 34° 8.194' E | 73 | 61 |
| | 10° 35.400' S | 34° 8.248' E | 129 | 39 |
| | | | 120 | 52 |

2) Table of Bedding Orientations

| Domain | Latitude | Longitude | Strike (°) | Dip (°; RHR) |
|---|---|---|---|---|
| C | 9° 56.141' S | 33° 44.695' E | 80 | 6 |
| | | | 13 | 15 |
| | 9° 56.642' S | 33° 45.195' E | 330 | 30 |
| | | | 338 | 25 |
| | | | 348 | 22 |
| | | | 354 | 28 |
| | 9° 56.71' S | 33° 45.401' E | 347 | 51 |
| | 9° 56.525' S | 33° 45.626' E | 346 | 27 |
| | | | 349 | 40 |
| | 9° 56.526' S | 33° 45.627' E | 12 | 17 |
| | 9° 56.512' S | 33° 45.946' E | 345 | 29 |

| | | | | |
|---|---|---|---|---|
| | 9° 56.652' S | 33° 46.410' E | 26 | 16 |
| | 9° 56.149' S | 33° 46.620' E | 318 | 17 |
| | | | 302 | 17 |
| | | | 282 | 25 |
| | 9° 57.115' S | 33° 50.064' E | 325 | 21 |
| D | 10° 3.516' S | 33° 49.369' E | 314 | 33 |

3) Table of Shear Zones

| Domain | Latitude | Longitude | S–Plane Strike (°) | S–Plane Dip (°; RHR) | C–Plane Strike (°) | C–Plane Dip (°; RHR) |
|---|---|---|---|---|---|---|
| A | 9° 45.343' S | 33° 39.798' E | 310 | 74 | 286 | 66 |
| | 9° 46.280' S | 33° 48.371' E | 322 | 81 | 309 | 77 |
| | | | 316 | 87 | 300 | 81 |
| | | | 322 | 85 | 288 | 80 |
| | | | 324 | 74 | 316 | 71 |
| | 9° 46.378' S | 33° 48.764' E | 313 | 79 | 291 | 84 |
| C | 9° 56.498' S | 33° 51.036' E | 343 | 83 | 174 | 74 |
| | 9° 56.588' S | 33° 51.086' E | 120 | 36 | 111 | 54 |
| D | 10° 3.516' S | 33° 49.369' E | 343 | 83 | 174 | 74 |
| F | 10° 20.482' S | 34° 11.444' E | 106 | 56 | 112 | 39 |

4) Table of Fault Orientations

| Dom-ain | Latitude | Longitude | Strike (°) | Dip (°; RHR) | Stria-tions | Displa-cement (cm)* | Length (m)* | Sense** |
|---|---|---|---|---|---|---|---|---|
| A | 9° 46.280' S | 33° 48.371' E | 39 | 44 | | | | Normal |
| | | | 25 | 41 | | | | Normal |
| | | | 47 | 65 | | | | Normal |
| | | | 47 | 65 | | | | Normal |
| | | | 45 | 62 | | | | Normal |
| | | | 46 | 68 | | | | Normal |
| | | | 29 | 38 | | | | Normal |
| | | | 40 | 54 | | | | Normal |
| | | | 39 | 59 | | | | Normal |
| | | | 41 | 52 | | | | Normal |
| | | | 47 | 59 | | | | Normal |

| | | | | | | | |
|---|---|---|---|---|---|---|---|
| | | | 290 | 84 | | | Unknown |
| | 9° 46.453' S | 33° 49.106' E | 191 | 57 | | | Normal |
| | | | 359 | 40 | | | Normal |
| | | | 13 | 41 | | | Normal |
| | | | 357 | 58 | | | Normal |
| | | | 36 | 78 | | | Normal |
| | | | 34 | 71 | | | Normal |
| | | | 27 | 66 | | | Normal |
| | | | 26 | 63 | | | Normal |
| | | | 35 | 67 | | | Normal |
| | | | 34 | 66 | | | Normal |
| | | | 23 | 60 | | | Normal |
| | | | 34 | 68 | | | Normal |
| | | | 29 | 70 | | | Normal |
| | | | 31 | 73 | | | Normal |
| | | | 3 | 50 | | | Normal |
| | | | 40 | 68 | | | Normal |
| | | | 25 | 60 | | | Normal |
| | | | 30 | 59 | | | Normal |
| | | | 33 | 55 | | | Normal |
| | | | 41 | 77 | | | Normal |
| B | 9° 53.530' S | 33° 33.476' E | 203 | 34 | | 20 | Reverse |
| | 9° 53.619' S | 33° 33.731' E | 116 | 80 | | 50 | Normal |
| | | | 160 | 71 | | 10 | Normal |
| | | | 145 | 52 | | 10 | Normal |
| | 9° 53.654' S | 33° 33.880' E | 231 | 38 | | | Reverse |
| | | | 345 | 61 | | 25 | Normal |
| | | | 165 | 80 | | 5 | Normal |
| | | | 338 | 67 | | 3 | Reverse |
| | 9° 53.847' S | 33° 34.238' E | 201 | 34 | | 10 | Reverse |
| | | | 170 | 55 | | 10 | Normal |
| | | | 169 | 57 | | 10 | Normal |
| | | | 185 | 54 | | 50 | Normal |
| | | | 70 | 52 | | | Reverse & Right Lateral |
| | | | 150 | 55 | 54, 085 | 5 | Normal |

| | | | | | | | | |
|---|---|---|---|---|---|---|---|---|
| | 9° 54.359' S | 33° 34.826' E | 34 | 74 | | 30 | | Normal |
| | | | 220 | 67 | | | | Normal |
| | 9° 53.816' S | 33° 36.558' E | 108 | 64 | | 10 | | Normal |
| | | | 57 | 15 | | 10 | | Normal |
| C | 9° 56.730' S | 33° 50.579' E | 197 | 39 | | 5 | 1 | Reverse |
| | | | 244 | 46 | | 15 | 7 | Oblique & Left Lateral |
| | | | 10 | 12 | | 5 | 10 | Reverse |
| | | | 290 | 28 | | 20 | 2 | Reverse |
| | | | 5 | 32 | | 5 | 2 | Reverse |
| | | | 310 | 14 | | 8 | 12 | Reverse |
| | | | 55 | 64 | | 5 | 8 | Reverse |
| | | | 44 | 18 | | 5 | 8 | Reverse |
| | | | 15 | 16 | | 10 | 9 | Reverse |
| | 9° 56.508' S | 33° 50.838' E | 358 | 66 | | | | Unknown |
| | | | 275 | 65 | | | | Unknown |
| | | | 12 | 72 | | | | Unknown |
| | 9° 56.498' S | 33° 51.036' E | 162 | 81 | 76, 191 | | | Normal |
| | 9° 55.575' S | 33° 44.261' E | 224 | 68 | | 10 | 10 | Reverse |
| | | | 24 | 27 | | 2 | 3 | Normal |
| | | | 226 | 73 | | 5 | 10 | Reverse |
| | | | 222 | 68 | | 3 | 10 | Reverse |
| | | | 230 | 74 | | 2 | 10 | Reverse |
| | 9° 55.766' S | 33° 44.292' E | 26 | 3 | | 10 | 10 | Reverse |
| | | | 26 | 3 | | 10 | 10 | Reverse |
| | | | 49 | 13 | | 15 | 10 | Reverse |
| | | | 218 | 64 | | | | Unknown |
| | 9° 56.037' S | 33° 44.545' E | 200 | 54 | | | | Unknown |
| | | | 288 | 43 | | 5 | 5 | Reverse |
| | | | 122 | 60 | 46, 260 | | | Unknown |
| | 9° 56.141' S | 33° 44.695' E | 16 | 77 | | 5 | 12 | Normal |
| | | | 26 | 72 | | 15 | 5 | Reverse |
| | | | 28 | 76 | 73, 125 | 100 | 15 | Normal |

| | | | | | | | | |
|---|---|---|---|---|---|---|---|---|
| | 9° 56.642' S | 33° 45.195' E | 184 | 77 | 79, 099 | | | Reverse |
| | | | 190 | 87 | 85, 080 | | | Reverse |
| | | | 191 | 68 | 66, 104 | | | Reverse |
| | | | 203 | 68 | | | | Normal |
| | | | 358 | 78 | 74, 124 | | | Normal |
| | | | 173 | 52 | | | | Reverse |
| | 9° 56.71' S | 33° 45.401' E | 205 | 37 | | 10 | | Normal |
| | | | 159 | 67 | | 20 | | Reverse |
| | 9° 56.526' S | 33° 45.627' E | 179 | 77 | | 2 | 7 | Reverse |
| | | | 165 | 53 | | | | Unknown |
| | | | 0 | 61 | | 20 | | Normal |
| | | | 163 | 54 | | | | Unknown |
| | 9° 56.652' S | 33° 46.410' E | 130 | 52 | | 300 | 12 | Normal |
| | 9° 55.911' S | 33° 46.904' E | 314 | 37 | | | | Unknown |
| | 9° 57.225' S | 33° 47.756' E | 75 | 71 | | 10 | 8 | Normal |
| | | | 280 | 73 | | 100 | 10 | Normal |
| D | 10° 1.298' S | 33° 55.922' E | 202 | 68 | | | | Thrust |
| | 10° 3.516' S | 33° 49.369' E | 1 | 80 | | | | Normal |
| | | | 202 | 77 | | | | Normal |
| | | | 202 | 83 | | | | Normal |
| | | | 194 | 75 | | | | Normal |
| | | | 342 | 84 | | 2 | | Normal |
| | | | 4 | 81 | 72, 121 | | | Normal |
| | | | 194 | 77 | | | | Normal |
| | | | 352 | 85 | | 3 | | Normal |
| | | | 188 | 74 | | | | Normal |
| | | | 1 | 77 | | | | Normal |
| | | | 5 | 84 | | | | Normal |
| E | 10° 18.376' S | 34° 4.343' E | 126 | 43 | 37, 229 | | | Normal |
| | | | 105 | 43 | 47, 187 & 39, 180 | | | Normal |
| F | 10° 25.673' S | 34° 14.661' E | 173 | 69 | 64, 286 | | | Normal |
| | | | 196 | 70 | | | | Normal |

| | | | | | | |
|---|---|---|---|---|---|---|
| | | | 125 | 47 | | Normal |
| | | | 90 | 74 | 72, 190 | Normal |
| | | | 71 | 76 | | Normal |
| G | 10° 35.700' S | 34° 8.673' E | 55 | 71 | | Unknown*** |
| | | | 98 | 79 | | Unknown*** |
| | | | 75 | 74 | 24, 244 | Unknown*** |
| | | | 162 | 50 | | Unknown*** |
| | 10° 35.482' S | 34° 8.174' E | 59 | 68 | 69, 154 | Unknown*** |

*Any unlisted fault lengths should be assumed to be outcrop-scale. Any unlisted fault displacement means that we could not determine this value.
**Sense was determined by examining fault stepping and relative motion of offset bedding or foliations
***While the faults in Domain G did not display any sense of movement indicators, the large damage zones and context from the regional geology led us to believe these were normal faults. They were plotted as such in Figure 14.

VITA

Sam Michael Dawson

Candidate for the Degree of

Master of Science

Thesis: THE INFLUENCE OF THE MUGESE SHEAR ZONE STRUCTURES ON STRAIN ACCOMMODATION IN THE NORTHERN MALAWI RIFT

Major Field: Geology

Biographical:

Education:

Completed the requirements for the Master of Science in Geology at Oklahoma State University, Stillwater, Oklahoma in December, 2016.

Completed the requirements for the Bachelor of Science in Geology at The University of North Carolina at Chapel Hill, Chapel Hill, NC in 2014.

Experience:

OSU Head Graduate Teaching Assistant – Physical Geology for Science Majors
Geophysical and Structural Field Work in Malawi
Concho Resources – Geoscience Internship

Professional Memberships:

AAPG Student Member
AGU Student Member